~~Application of the creeping flow restoration method~~ What does it take to ~~an analogue model~~restore geological models with "natural" boundary conditions ?

Melchior Schuh-Senlis[1], **Guillaume Caumon**[1], **and Paul Cupillard**[1]

[1]RING, GeoRessources / ENSG, Université de Lorraine / CNRS, F-54000 Nancy

Correspondence: Melchior Schuh-Senlis (melchiorschuh@gmail.com)

Abstract.

Structural restoration is commonly used to assess the deformation of geological structures and to reconstruct past basin geometries. ~~For this, most methods use numerical simulations to compute the deformation of geological models from a chosen deformation mechanism for each geological layer, and conditions applied on the boundaries depending on geological knowledge. For example, geomechanical restoration classically uses elastic motion, considers faults as frictionless contact surfaces, and imposes boundary conditions such as interface flattening to estimate the paleo-deformation. To bring more physical behavior and better handle large deformations~~Classically, restoration is formulated as a geometric or mechanical problem driven by geometric boundary conditions to flatten the top surface. This paper investigates the use of boundary conditions in restoration to better approach the actual mechanical processes driving geological deformations. For this, we use a reverse time Stokes-based method with negative time step advection. ~~In order to test the method on complex models including various rheology and faults~~To be able to compare the results of the restoration to known states of the model, we apply it to ~~an analogue experimentmodel. We first show that reasonable restored geometries can be obtained using classical kinematic boundary conditions~~ a model based on a laboratory analogue experiment. In the study, we first test the behavior of the restoration process with Dirichlet boundary conditions such as those often used in geomechanical restoration schemes. We then ~~show that it is possible to relax the imposed kinematic conditions and replace them by more physical boundary conditions . These conditions, however, imply~~ relax these boundary conditions by removing direct constraints on velocity, replace them with more ‘natural’ conditions such as Neumann and free surface conditions, and measure the horizontality of the free surface as a restoration criterion. The proposed boundary conditions confer a larger impact of the material properties on the restoration results. ~~Finally, we show that relaxing the boundary conditions and using the previous imposed conditions as choice criteria allows both the assessment of the value of the~~ The choice of appropriate effective material properties ~~, and the improvement of the restoration results~~is, therefore, necessary to restore structural models without kinematic boundary conditions.

---

1 Introduction

~~The Earth’s subsurfaceis the result of millions of years of deformation. As available datacovers at best a few decades, reconstructing the deformation history from the current geometry of a geological region has been a concern for geoscientists. Restoration is an ensemble of methods which aim at this reconstruction by reversing the various processes that have taken place (e.g., Chamberlin, 1910; Dahlstrom, 1969). It covers different procedures and methodologies. The classical techniques in basin analysis are unfolding and unfaulting using length/area preservation in order to remove the effects of tectonic forces. In addition to this, several methods have been developed to take into account the effects of other important parameters, like~~ When studying the subsurface, geologists are faced with the sparsity of available data, and need to make assumptions based on their knowledge to fill the gaps between the observations. Structural restoration, which aims at reversing the tectonic deformations, was first introduced as a method to balance cross sections and characterize shortening (e.g., Chamberlin, 1910; Dahlstrom, 1969; Schönborn, 1999). More recently, the approach evolved to assess the tectonic evolution through time (e.g., Back et al., 2008; de Melo Garcia et al., 2012; Espurt et al., 2019; Crook et al., 2018) or to assess the localization of deformation (e.g., Al-Fahmi et al., 2016b; Chauvin et al., 2018). Various methods were also developped to add more complexity and study different geological and physical aspects, such as erosion and deposition of sediments (e.g., Dimakis et al., 1998), isostasy compensation (e.g., Allen and Allen, 2013), thermal subsidence due to mantle thermal effect (Royden and Keen, 1980; Allen and Allen, 2013), rock decompaction due to a change of load (e.g., Athy, 1930; Durand-Riard et al., 2011; Allen and Allen, 2013), or, at a smaller scale, the erosion and deposition of channelized systems (e.g., Parquer et al., 2017). ~~These methods allow us to generate paleo-basin geometries consistent with present-day observations for use in more elaborate hydro-mechanical forward models (e.g., Bouziat et al., 2019).~~ In this article, we focus on ~~the structural restoration based on~~ structural restoration aiming at unfolding and unfaulting.

~~Since the beginning of the last century, different~~ Various numerical methods have been ~~used for unfolding and unfaulting models, which can be classified in three categories~~developped for structural restoration, each using different deformation mechanisms. The first ~~category uses~~ implementations used geometric and kinematic rules (e.g., Chamberlin, 1910; Dahlstrom, 1969; Gratier, 1988; Rouby, 1994; Groshong, 2006; Lovely et al., 2018; Fossen, 2016). ~~The first implementations in two dimensions (2D) used balanced restoration (e.g., Chamberlin, 1910; Dahlstrom, 1969; Groshong, 2006). Later on, 2.5D methods such as map restoration (e.g., Cobbold and Percevault, 1983; Rouby, 1994; Ramón et al., 2016) and finally three dimensional (3D) geometrical methods were proposed (Massot, 2002; Muron, 2005; Lovely et al., 2018), allowing the tracking of internal volumetric deformation. These methods~~Numerous authors, however, ~~considerably simplify rock deformation mechanisms, ignore mechanical layering effects and are extremely limited when considering salt basins. In this light, numerous authors have stressed out the necessity of incorporating more physical principles into the restoration of geological models~~ stressed out their lack of physical principles and their limitations in cases such as salt basins (Fletcher and Pollard, 1999; Ismail-Zadeh et al., 2001; Muron, 2005; Maerten and Maerten, 2006; Moretti, 2008; Guzofski et al., 2009; Al-Fahmi et al., 2016a).

~~In order to add some mechanical concepts in the restoration process, the second category of methods considers the restoration of sediment layersassumed to deform elastically between frictionless fault surfaces. It has been developed since the 2000s as a geomechanical simulation with specific boundary conditions (Maerten and Maerten, 2001; De Santi et al., 2002; Muron, 2005; Moretti et al., 2006; Maerten and Maerten, 2006; Guzofski et al., 2009;~~

Methods using geomechanical simulations were then developped, taking into account the material behavior inside the geological layers, and applying a set of conditions to restore the models. In this approach, internal deformation is not known *a priori*; it is determined from the input mechanical behavior of rocks and the applied boundary conditions. ~~The model is parameterized with elastic properties and the displacement is computed by solving the equation of motion, in which the Cauchy stress tensor is defined by Hooke's law. The restoration itself is performed by the specific boundary conditions constraining the model. These conditions, usually imposed on the displacement, rely on assumptions made from the geological knowledge, such as: the uppermost horizon was flat and horizontal at deposition time and it was not faulted (Chauvin et al., 2018). Although these methods offer significant advances in the structural restoration of geological models, the boundary conditions set to unfold and unfault the medium are unphysical as the imposed depth of the free surface is the main driver of the deformation (Lovely et al., 2012; Chauvin et al., 2018). As a result, this restoration approach has overcome some limitations of the geometric restoration process, but it still needs to be improved to better account for different rheologies, larger deformations, faults, salt tectonics, and boundary conditions.~~

~~The last category of methods was introduced in 1999 as a way to improve the restoration of salt structures (Kaus and Podladchikov, 2001; Ismail-Zadeh et al., 2001, 2004; Ismail-Z. It relies~~ For example, in the presence of salt structures, methods based on considering the rocks as viscous fluids ~~to compute the motion, and on applying negative time steps. It is motivated both~~ were introduced (Kaus and Podladchikov, 2001; Ismail-Zadeh et al., 2001, 2004; Ismail-Z. In these methods, the motion is computed using highly viscous fluid mechanical laws inside the stratigraphic units and their behavior under their own weight. This is motivated by the fact that rock salt and some sediment overburdens behave as viscous fluids over time scales of millions of years, and by the reversibility of the Stokes equations~~, which allows the backward timestepping. The first implementations used a linear viscous (Newtonian) rheology to restore 2D seismic cross-sections of salt diapirs (Ismail-Zadeh et al., 2001), and 3D Rayleigh-Taylor instabilities (Kaus and Podladchikov, 2001; Ismail-Zadeh et al., 2004). Since then, the method has been used for 3D unfolding in the absence of gravity (e.g., Schmalholz, 2008), extended to non-linear (power-law) viscous behavior (e.g., Lechmann et al., 2010; Fernandez, 2014), or used to study the reverse modelling of flanking structures (e.g., Kocher and Mancktelow, 2005). Schuh-Senlis et al. (2020) have shown~~. At this point, however, faults have been neglected in most of these restoration methods, or only in numerical test-cases (e.g., Schuh-Senlis et al., 2020). Many authors have also proposed to use linear elastic behavior and frictionless faults

(Maerten and Maerten, 2001; De Santi et al., 2002; Muron, 2005; Moretti et al., 2006; Maerten and Maerten, 2006; Guzofski et al., 2009; . These elastic restoration methods classically rely on boundary conditions that impose the uppermost horizon as flat, horizontal and unfaulted at deposition time. The issue here is that while geological assumptions can give an idea of the total displacement that should happen, its discretization in time is unknown. As such, the validity and the ability of these boundary conditions to replace the tectonic forces applied on forward geologic deformation has been questioned (e.g., Lovely et al., 2012; Chauvin et al., 2018) . In particular, Chauvin et al. (2018) show that a lateral kinematic boundary condition can be required for increasing the accuracy of elastic restoration. Schuh-Senlis et al. (2020) show the possible extension of the viscous fluids restoration method to sedimentary basins including faults~~and a non-flat top surface~~ , and using less constraining boundary conditions, relying on a free surface on top and the weight of the materials to drive the restoration process. However, they considered only synthetic models ~~,~~ generated using the same software, physical laws and material parameters for both the forward and the backward simulations.

~~Considering these methods as a whole, they can be regrouped as numerical simulations which try to restore a model to a previous state in its history. In these simulations, a specific rheology is used to simulate how layers react to surrounding deformation, and specific boundary conditions are used to drive the model deformation. The main issue, in general, is then that the paleo-state of a geological model is not available, so checking the results of the simulations remains problematic~~In this paper, we investigate the complexity of restoring more complex structural model obtained from an analogue, gravity-driven, laboratory experiment, without imposing any boundary condition on the free surface. In this approach, the free surface horizontality will not be imposed, but used as a criterion to check the restoration quality. We build on the method of Schuh-Senlis et al. (2020) and use the same creeping flow restoration process. The simulations done in this article also use the Particle-In-Cell implementation in the FAIStokes code of Schuh-Senlis et al. (2020). Creeping flow restoration is chosen here for three main reasons. First, the deformation inside the model is driven by gravity and backward time-stepping. Second, it can handle the rheology of viscous layers (such as salt layers in geological models). Third, it allows the faults to be considered as shear bands with a lower viscosity instead of frictionless surfaces.

~~Analogue modeling tries~~To increase the knowledge on the previous states of the restored model, and be able to compare the restoration results with these states, we use an analogue experiment model as a test-case. The purpose of analogue modeling is, with forward experiments, to find the paleo-deformations leading to specific geological structures (Hall, 1815; Ramberg, 1981; Willis, 1894; Cobbold et al., 1989). The idea is to choose materials that present the same deformations as those observed in geological models, but are sufficiently weak to deform at laboratory scales. For example, the experiment presented hereafter in the article has a size around 30 cm × 5 cm and lasts about 3 hours, but the properties of its materials are such that its deformation is similar to that of a sedimentary basin several kilometers wide, over several hundreds of thousands of years. As a result, analogue experiments produce structural models where not only the post-deformation state, but also the paleo-state and the deformations ~~the model underwent~~ undergone by the model are known. For this reason, several studies have used them to assess the results of numerical schemes, both forward (e.g., Buiter et al., 2016; Schreurs et al., 2016) and backward (e.g., Chauvin et al., 2018).

~~In this paper, we investigate the application of the creeping flow restoration to such an analogue laboratory experiment model, including faults and a deformed top surface. The simulations done in this article used the Particle-In-Cell implementation in the FAIStokes code of Schuh-Senlis et al. (2020). Creeping flow restoration is chosen here for three main reasons. First, the deformation is driven by gravity and backward time-stepping, which is assumed more physical. Second, it can handle the rheology of salt layers. Third, it allows the faults to be considered as shear bands with a lower viscosity instead of frictionless surfaces. This allows of change of paradigm from classical restoration schemes trying to impose boundary conditions and rheologies in the restoration simulations. Indeed, the aim of this paper is to show that it is possible to relax the boundary conditions of the simulations, and use the geological knowledge not as conditions but as criteria to check the restoration quality and find the effective material properties in the restored model.~~

The outline of this paper is as follows: we first ~~present~~ review the concepts of Stokes flow-based restoration and the ~~workflow of the FAIStokes code in which we implement it~~FAIStokes implementation used in this study. In a second part, we present the analogue experiment which was used, and the numerical model created from it. In a third part, we start by restoring this model using ~~kinematic boundary conditions~~ boundary conditions which impose the deformation of the model, and then ~~introduce new boundary conditions that may add more physical meaning to the restoration. Finally, we use these boundary conditions~~ replace them one by one to remove the kinematic dependance. For this, we introduce lateral boundary conditions which aim at better approaching the local stress state, and remove the boundary condition on the top surface to leave it free. These boundary conditions, however, stress the importance of the material properties in the model, and the inability of the method to restore the model properly without proper effective material properties. In a last part, we show how the proposed boundary conditions could be used to assess the impact of the material parameters on the restoration, and ~~we show~~ how to find relevant values for them.

2 Method

2.1 Creeping flow restoration

2.1.1 Stokes flow equations

~~The standard equations for creeping flows are the Stokes equations , consisting~~ In sedimentary basins, the deformation of rocks over long periods of time can be modeled by viscous fluids, for which the deformation is described by the Navier-Stokes equations. In this case, however, we usually deal with materials that are highly viscous (with a viscosity η over 10^{17} Pa.s), over time scales of thousands to millions of years. The inertial part of the Navier-Stokes equations can then be neglected, and the deformation is described by the Stokes equations for creeping flow (Massimi et al., 2006) . These equations consist of the momentum conservation equation

$$\nabla \cdot \boldsymbol{\sigma} + \boldsymbol{f} = \boldsymbol{0} \tag{1}$$

and the mass conservation equation for incompressible fluids (continuity equation)

$$\nabla \cdot \boldsymbol{v} = 0, \tag{2}$$

where ∇ is the del operator, $\boldsymbol{\sigma}$ is the stress tensor, $\boldsymbol{f}$ is the specific body force (usually the volumetric weight $\rho \boldsymbol{g}$), and $\boldsymbol{v}$ is the velocity. The stress consists of a deviatoric part $\boldsymbol{\tau}$ and an isotropic pressure p:

$$\boldsymbol{\sigma} = \boldsymbol{\tau} - p\mathbf{I}, \tag{3}$$

where $\mathbf{I}$ is the identity tensor. In the viscous flow assumption, the deviatoric part of the stress is

$$\boldsymbol{\tau} = 2\eta\mathbf{D}, \tag{4}$$

with η the dynamic viscosity and $\mathbf{D}$ the infinitesimal strain rate tensor defined by

$$\mathbf{D} = \frac{1}{2}\left[\nabla \boldsymbol{v} + (\nabla \boldsymbol{v})^T\right]. \tag{5}$$

Assembling Eq. (1), (3), (4), and (5), the momentum conservation equation can be written

$$\nabla \cdot \left[\eta(\nabla \boldsymbol{v} + (\nabla \boldsymbol{v})^T)\right] - \nabla p = -\rho \boldsymbol{g}. \tag{6}$$

~~In sedimentary basins, we usually deal with materials that are highly viscous (with a viscosity η over 10^{17} Pa.s), over time scales of thousands to millions of years, so these equations neglect the inertial part of the Navier-Stokes equations (Massimi et al., 2006). As such, the~~ These equations describe a steady-state flow and their resolution provides the velocity of a fluid at a specific position and time. When different fluids are present, the conditions that are applied at their boundaries, as well as their differences in density, can create instabilities such as Rayleigh-Taylor instabilities. These instabilities make the flow non-stationary as they advect the viscosity and density fields in time.

2.1.2 Backward advection

In forward simulation schemes, the Stokes equations (6) and (2) are solved for pressure and velocity, and the material representation of the geological model is advected from the velocity at each time step. The simplest way to do it is by using an Euler scheme, the position $\boldsymbol{x}(t+\Delta t)$ of a given point of the material model after a single time step being computed as

$$\boldsymbol{x}(t+\Delta t) = \boldsymbol{x}(t) + \boldsymbol{v}(t) \cdot \Delta t, \tag{7}$$

where $\boldsymbol{v}(t)$ is the computed velocity of the point at time t (while higher-order methods exist (e.g., Ismail-Zadeh and Tackley, 2010), particularly to stabilize the advection scheme in the case of large time steps, we choose to present the restoration idea with this order one approximation for simplicity). This Finite-Difference approximation relies on the idea that the chosen time step Δt is small enough to approximate the velocity of a particle as a constant over this time step (Δt is usually calculated using a Courant-Friedrichs-Lewy (CFL) condition (Courant et al., 1928)). Since the Stokes equations are linear and do not depend on previous time steps for the computation of the velocity, we can extend this approximation to backward simulations. This is the basis of backward time stepping restoration schemes: instead of applying Eq.(7), we apply

$$\boldsymbol{x}(t-\Delta t) = \boldsymbol{x}(t) - \boldsymbol{v}(t) \cdot \Delta t \tag{8}$$

for the advection of the points of the material model, at each time step, like in Fig. 1.

~~In this light, using viscous fluid properties instead of elastic properties to represent the mechanical behavior of geological materials holds several advantages, such as the use of boundary conditions that are closer to reality, like a free surface on top, or the account of other rheologies like a salt layer.~~

2.2 The FAIStokes code

The restoration scheme presented in the previous section has been implemented in the FAIStokes[1] code described by Schuh-Senlis et al. (2020). It relies on a Particle-In-Cell (PIC) scheme (e.g., Asgari and Moresi, 2012; Thielmann et al., 2014; Gassmöller et al., 2018, 2019; Trim et al., 2020), where the Stokes equations are solved using the Finite Element Method (FEM). ~~The general workflow of the code is~~

[1]**F**inite element **A**rbitrary Eulerian-Lagrangian **I**mplementation of **Stokes**

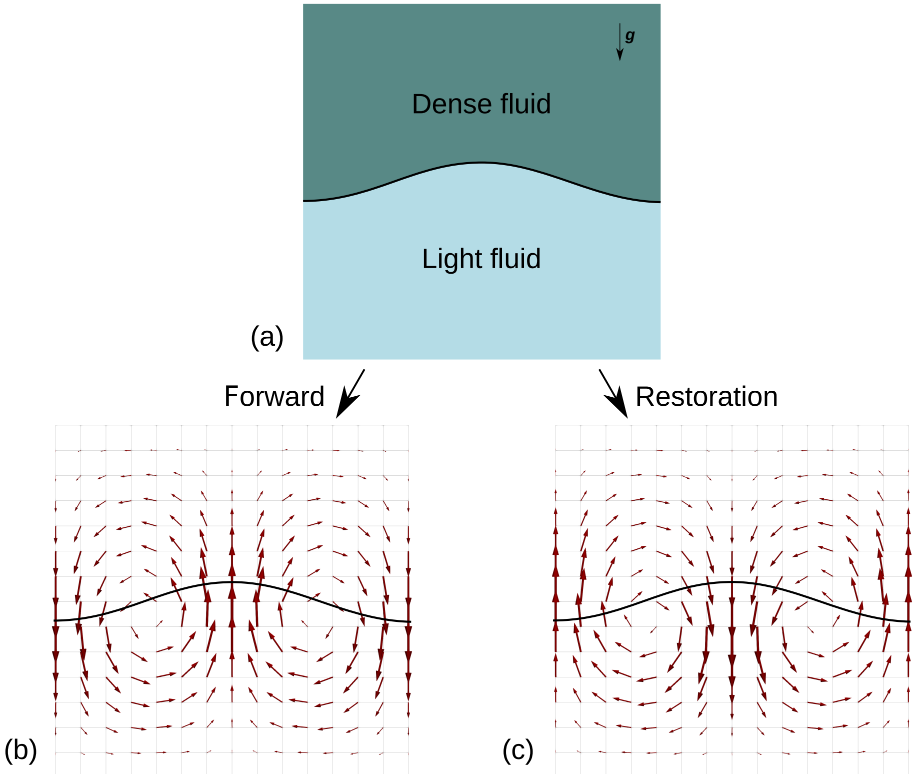

Figure 1. Example of the restoration scheme for a simple setup (a): as the arrows in (b) represent the velocity computed at a specific time step for a forward scheme, the advection of the material model in a restoration scheme is done with the opposite of the computed velocity, shown in (c).

shown in Fig. ??, and we here recall its main characteristics We here recall the main characteristics of the code.

Schematic workflow of the FAIStokes code structure. The pre-refinement step occurs at the beginning of the simulation (or during a reinitialization of the grid) to ensure that the velocity used for the advection step is computed using the adaptively refined grid.

2.2.1 Material discretization

During mechanical simulations, the material properties inside the model are tracked using particles; each of these particles discretizes the small part of the model around it and its properties. At each time step, the material properties of the particles are interpolated from the particle swarm to the FEM grid in order to build the stiffness matrix and its preconditioner. They are then used to solve the Stokes equations, for the velocity, on the grid. Following this, the particles are advected using the solution on the grid.

2.2.2 Viscosity model

During the experiments, we assume the materials to be linear viscous fluids with constant viscosity. While the viscosity of materials is known to vary with the temperature, we do not solve the heat transport equation here. Indeed, in sedimentary basins the temperature is mostly studied for the maturation of source rocks, but is not assumed to have sufficient variations to impact the viscosities on our scale. Additionally, the analogue laboratory experiment considered in this study (Section 3) was performed at room temperature.

2.2.3 Finite Element discretization

In FAIStokes, the Stokes equations are solved on a 2D grid using the FEM algorithms of the deal.II library (Bangerth et al., 2007; Arndt et al., 2019, 2020). Quadrilateral Taylor-Hood $Q_2 \times Q_1$ elements, satisfying the Ladyzhenskaya-Babuška-Brezzi (LBB) condition for stability (Donea et al., 2004), are used. The heat transport equation is not solved.

2.2.4 Grid and solvers

The grid and solvers come from the deal.II code. In the right-hand side of Eq. (6), the norm of the gravity vector $\boldsymbol{g}$ of is always $9.81\ \mathrm{m.s^{-2}}$ in our simulations, and its direction can be modified to introduce a tilt in the model. The matrix system is solved using an iterative FGMRES solver preconditioned by a block matrix involving the Schur complement

(Kronbichler et al., 2012). The grid is adaptively refined and coarsened using deal.II's features, based on the position of the faults and the viscosity variability in the elements. An Arbitrary Lagrangian Eulerian (ALE) scheme is also applied on the grid, as explained in the next paragraphs.

2.2.5 Velocity interpolation

Once the Stokes equations are solved in the domain, the velocity is interpolated on the particle swarm using a Q_2 interpolation scheme. Depending on whether the simulation is forward or backward, the displacement of each particle is computed using either Eq. (7) or (8). The value of the time step Δt is determined from the CFL condition. Finally, the advection is done with a 2^{nd}-order Runge-Kutta scheme in space.

2.2.6 Top surface displacement

During the simulations, the top surface of the model coincides with the top of the computation grid, meaning there is no volume between them. The boundary conditions on this interface are then applied directly to the nodes at the top of the grid. The top surface and model interfaces are tracked by ~~separate point swarms~~ sets of passive tracers in the simulations ~~. These point swarms are denser~~ with an initial horizontal spacing ten times lower than the material ~~particle swarm and are one dimension lower (i.e. lines in our 2D cases)~~particles spacing. They are advected at each time step the same way as the particle swarm that represents the model. After its displacement or during the setup of the grid, the point swarm discretizing the top surface is used as a reference to move vertically the nodes of the grid at the top of the model, so that they match the top surface. This vertical displacement is then propagated to the rest of the grid. The free surface stabilization algorithm proposed by Kaus et al. (2010) is used in all the simulations which consider the top surface as a free surface.

3 Presentation of the analogue model

~~The model we use in this article~~

3.1 Analogue experiment description

The analogue model used in this study comes from the deformation of a structural sandbox experiment made by IFPEN[2] and C&C Reservoirs[3], 2016, DAKS ™ (Digital Analogs Knowledge System). This experiment aimed to reproduce gravity-driven extensional passive margin structures overlaying a salt layer (Fig. 2). The experiment setup is shown in Fig. 4 and presented hereafter.

[2]https://www.ifpenergiesnouvelles.fr

[3]https://www.ccreservoirs.com

Two initial layers were deposited in the model box, forming the pre-growth strata: a layer of 18 mm of silicone SMG 36 and a layer of 4 mm of sand. On the right-hand side, no boundary was set, while walls were present on the three other sides to prevent the material from moving other than vertically on these interfaces. The model box was then inclined with a 1.5° angle to simulate a basinward tilt, inducing natural gravity-driven extension towards the right-hand side. The experiment lasted for 256 minutes, during which 12 new layers of alternatively pyrex and sand were deposited to simulate stratigraphic growth. This deposition was made in stages, at specific time intervals of between 10 and 18 minutes, shown in Table 2. These new layers flattened the topography by filling the depressions. The ~~model resulting from the experiment was analyzed using X-ray tomography. This method allows the computation of cross-sections without physically cutting the model. As it is non-destructive, it does not need the consolidation of the model beforehand and avoids the deformation that could occur during the cutting. Moreover, it is dynamic, so it can be used to track the evolution of the experiment. The differentiation of the layers in the cross-sections is done using the difference in density and X-ray attenuation. In our numerical experiments, we made the choice of working at laboratory scale (width of 280 mm and duration of 256 minutes), and we used the known silicone viscosity to reduce the number of parameters to test.~~

~~Setup of the creation of the laboratory analogue model. A layer of 18 mm of silicone and a layer of 4 mm of sand are first deposited on a slab with an open boundary. The slab is then tilted with an angle $\theta = 1.5°$, and the layers start to deform with gravity in the direction of the open boundary. During the 256 minutes of the experiment, 12 new layers of alternatively pyrex and sand are deposited, flattening the topography and simulating stratigraphy growth.~~

3.2 ~~Available data~~

~~Various data are available for this analogue experiment. First, the experiment setup is given, as shown in Fig. 2. Second, the physical~~ basal silicone material, with a viscous fluid behavior, aims at representing a basal salt layer. The sand and pyrex layers represent clastic sedimentary deposits. The properties of the silicone, sand and pyrex layers are ~~known (~~shown in Table 1~~)~~. ~~Third,~~

3.2 Analysis of the experiment using X-ray tomography

The model resulting from the experiment was analyzed using X-ray computed tomography (CT). This method allows the computation of cross-sections without physically cutting the model. As CT is non-destructive, it does not need the consolidation of the model beforehand and avoids the deformation that could occur during the cutting. CT is

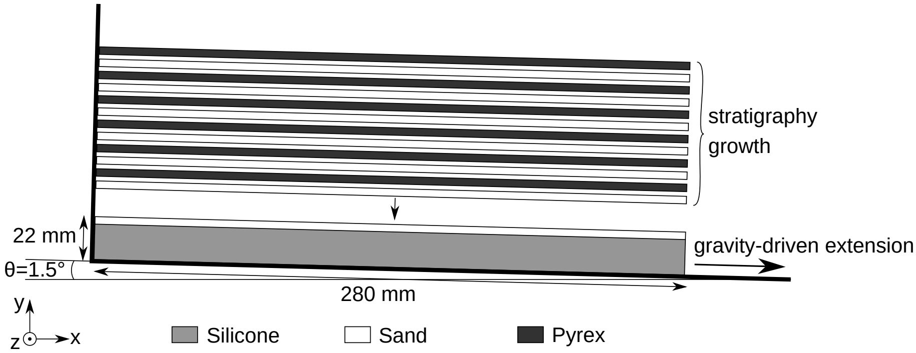

Figure 2. Setup of the creation of the laboratory analogue model from IFPEN and C&C Reservoirs.

Table 1. Physical properties of the silicone, sand and pyrex layers for the analogue experiment. ~~In dark red, the properties that are not relevant due to the difference in rheology between brittle and ductile layers.~~ From ~~the IFPEN documentation on the analogue model experiment (IFP and C&C Reservoirs, 2006)~~IFP and C&C Reservoirs (2006).

Physical properties	Sand	Pyrex	Silicone SGM36
Rheological ~~behaviour~~ behavior	Brittle		Ductile (Newtonian)
Density	1.3 - 1.5	1.2	0.97
Grain size (μm)	100-120	80-120	Not applicable
Internal friction angle	40°	32-36°	Not applicable
Cohesion (mPa)	0.001-0.002	> 0.005	Not applicable
Viscosity (Pa.s)	Not applicable		5.10^4
Natural analogue	brittle rocks (sandstones, limestones)		ductile rocks (salt, undercompacted shales)

also fast enough to be used to track the evolution of the experiment. The differentiation of the layers in the cross-sections is done thanks to the difference of density and X-ray attenuation. The X-ray tomography images ~~are available; they~~ have been taken every two minutes and their resolution is 0.62 mm per pixel. As X-ray tomography is sensitive to density, layer interfaces can be hard to pinpoint where the density contrast is weak. ~~Moreover, no~~ No images have been taken during the deposition of sand and pyrex layers, so there are also small time gaps at these moments. These images, however, make it possible to determine both the times between each layer deposition in the forward (laboratory) experiment, as well as the height of the topography after the deposition of each layer (Table 2). The tomography images only cover the left part of the model, so the material flowing on the right-hand side of the model is not tracked. This also means that the velocity on the right-hand side of the model, and the total amount of extension, are not known.

In the present work, we use a cross-section taken at the end of the experiment (Fig. 3) to create an initial model on which to test our restoration method. While this implies working in 2D and therefore ignoring out-of-plane displacements, it reduces significantly the computation time for the restoration process, so that more tests on the impact of the different restoration settings can be performed.

3.3 Creation of the numerical model

To digitize the cross section in Fig. 3, we first rotate it left by 1.5° to horizontalize the model base and cut it to a rectangular shape. This eases the digitization process and allows for the easier construction of the computation grid around the model. A graphical user interface developed for FAIStokes is then used to digitize the interfaces and the faults in the cross-section. Finally, a particle swarm is created, and the fault and interface lines are used to define the layers and determine the material properties of the particles. The particle swarm contains 667 087 particles at the beginning of the restoration, with a distance of 0.14 mm between each particle. While the grid is adaptively refined, and the refinement and coarsening changes during the simulations, this ensures a minimum of 20 particles per cell during the simulation (for the most refined parts of the grid).

In the faults, the viscosity of the particles is taken minimal at the position of the fault line (representing the fault core), and increases with a power-law ~~until reaching the fault border. The distance between the fault core and the fault zone border, defining the~~ towards the boundary of the shear band, as inspired by Faulkner et al. (2006). The shear band thickness ~~,~~ is different for each fault (Table 3). Indeed, a close look to the cross-section in Fig. 3 shows that each fault has a different ~~range~~ width of deformation around its core.

Table 2. Duration of the restoration simulation and topography height after deposition of each layer of the analogue model. The indices of the layers are shown in Fig. 4.

Layer index	Simulation duration (minutes)	Topography height (mm)	Material
1	18	52.6	sand
2	12	50.06	pyrex
3	16	48.26	sand
4	16	45.71	pyrex
5	16	44.68	sand
6	14	42.38	pyrex
7	14	40.09	sand
8	12	38.55	pyrex
9	10	37.27	sand
10	18	33.7	pyrex
11	14	31.14	sand
12	16	26.8	pyrex
13	14	22	sand
14	(pre-growth layers)	18	silicone

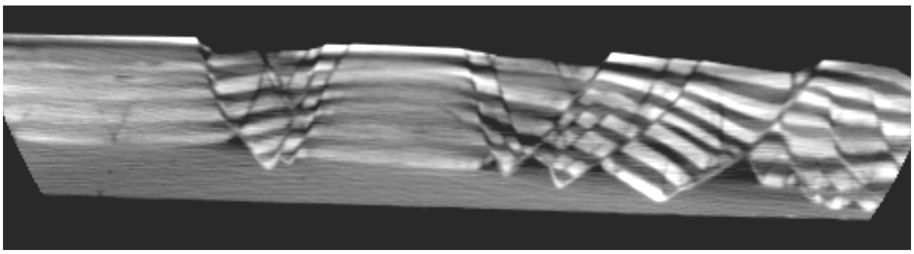

Figure 3. Final cross-section of the analogue experiment. The image has been obtained using X-ray tomography, with a resolution of 0.62 mm per pixel. As the range of the imaging is limited, the borders of the experiment are not present on the image. CT image from IFP and C&C Reservoirs (2006)

Table 3. Shear band thicknesses of the fault in the analogue model. The values come from the analysis of the final cross-section (Fig. 3). The index of each fault is given in Fig. 4. The faults with two values have a shear thickness that is reduced at the top of the model because they have a lower deformation range there.

Fault index	Shear band thickness (mm)
1	2.2
2	1.4
3	1.8
4	2.1
5	1.2-2
6	1.2-1.8
7	1.6-3
8	1
9	1
10	1
11	1
12	1.6
13	1
14	1.4
15	1

The obtained numerical model geometry input to the restoration process can be seen in Fig. 4. To restore it, the times between each layer deposition in the forward (laboratory) experiment are used as the restoration durations (Table 2) after which the particles at the top are stripped off. The X-ray tomography images are also used to determine the height of the topography after the deposition of each layer. This height is used, in some cases, to impose a flattening condition on the top surface of the model. Duration of the restoration simulation and topography height after deposition of each layer of the analogue model. The indices of the layers are shown in Fig. 4. Layer index Simulation duration (minutes) Topography height (mm) Material 1 18 52.6 sand 2 12 50.06 pyrex 3 16 48.26 sand 4 16 45.71 pyrex 5 16 44.68 sand 6 14 42.38 pyrex 7 14 40.09 sand 8 12 38.55 pyrex 9 10 37.27 sand 10 18 33.7 pyrex 11 14 31.14 sand 12 16 26.8 pyrex 13 14 22 sand 14 (pre-growth layers)18 silicone In the following numerical experiments, we assume that the model behavior can be approximated using creeping flow as well as geological models, not only in the silicone layer which is chosen to behave so, but also in the brittle and ductile sand and pyrex layers. As there is no inertial part in

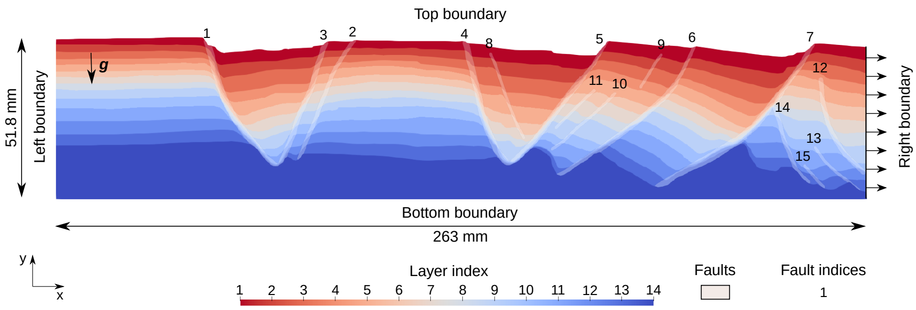

Figure 4. Setup of the analogue model to input in FAIStokes for the restoration simulations. The model boundary conditions are not specified here, as their choice and impact on the simulations are discussed in the next section. During the simulations, the tilt of the model is introduced by rotating the gravity vector, as explained in Section 2.2.4.

the deformation of the materials during the experiment, the Stokes approximation can be used. In this type of model, the compaction and decompaction of materials can be important, so we choose to focus on the first restoration step to avoid taking it into account. In the numerical experiments that follow, we make the choice of working at laboratory scale (width of 280 mm and duration of 256 minutes), and we use the known silicone viscosity to reduce the number of parameters to test.

4 Boundary condition analysisconditions for restoration

In geomechanical restoration, specific boundary conditions have been used, such as flattening the top surface or tying the fault lines applying specific deformation to remove fault throw (by tying the curves representing the footwall and hangingwall cutoff of horizon surfaces at faults for example) (Muron, 2005; Chauvin, 2017). Because viscous behavior cannot be handled by elastic motion, the interfaces with material, interfaces between brittle sediments and basal salt layers have usually been considered as free surfaces (e.g. Stockmeyer and Guzofski, 2014) (e.g., Stockmeyer and Guzofski, 2014). Here, we start with simple boundary conditions and show their impact on the motion deformation inside the modeland how they can be upgraded to . We then show how more physical assumptions . The material properties of the layers are not studied here (they will be covered in Section 5), so we consider them as constant in the simulations presented in this section(can be used to remove the kinematic part of these boundary conditions. In this section, the material properties described in Table 4)are used. The density of the layers comes from the data (Table 1), and the density of the particles inside the faults is assumed to be the same as in the rest of the layer they belong to. The viscosity of the silicone is known, and we set the viscosity of the sand and pyrex as ten times higher. The viscosity at the fault core is set to be the same as inside the silicone. The uncertainty of the viscosity of the sand, pyrex and fault cores will be adressed in Section 5). In all the following experiments, the left boundary condition is set to a free slip and the bottom boundary condition is set to a no slip.

4.1 Restoration using kinematic boundary conditions

The first boundary conditions we test are kinematic. The bottom and left boundariesare set to free slip, so the motion inside the model is driven both by gravity and by the velocity applied at the boundaries. For each layer, the top surface is flattened using a Dirichlet condition: the vertical component of the velocity on the top nodes of the grid at time t is set to

$$v_y(n,t) = -\frac{Y_{final} - y(n,t)}{T_{simulation} - t}, \qquad (9)$$

with n the index of the node, $y(n,t)$ its altitude, $T_{simulation}$ the duration of the restoration for the current top layer, and Y_{final} the height of the topography at the end of the restoration of the layer (determined from the tomography images and shown in Table 2). The velocity 9 computed in Eq. (9) is in the opposite direction of the final altitudeforward sense, as it is then applied with a backward advection scheme. The Following Chauvin et al. (2018), the right boundary is set to a fixed flow. As we consider incompressible flow, the kinematic conditions must ensure the conservation of model volume during the simulation. This means that the volume change due to the topography evolution ΔV_{top} must be compensated by the volume entering at the right boundary ΔV_{right}:

$$\Delta V_{top} = \Delta V_{right}. \qquad (10)$$

Using the CFL condition, the time step should be computed from the velocity field and change at each time iteration for the computation to be stable. This is an issue here, because ΔV_{top} depends on the time step (computed from the velocity field), and the horizontal velocity at the right boundary determined from ΔV_{right} is necessary for the computation of the velocity field. To get rid of this dependency, we impose a

Table 4. Material properties of the silicone, sand and pyrex layers in the restoration simulations ~~which assess the impact~~ of ~~different boundary conditions~~Section 4. ~~In red, the~~ The density of the particles inside the faults is the same as the density of the layer to which they belong. The ~~grey cells show the~~ values ~~that come~~ coming from the laboratory experiment are indicated.

Material properties	Sand	Pyrex	Silicone SGM36	Fault core
Density	1.4 (laboratory)	1.2 (laboratory)	0.97 (laboratory)	Layer density
Viscosity (Pa.s)	5.10^5	5.10^5	5.10^4 (laboratory)	5.10^4

fixed time step Δt such that the volume change is constant:

$$\Delta V_{top} \simeq \frac{V_f - V_i}{T_{simulation}} \Delta t = \text{constant}. \tag{11}$$

The horizontal flow at the right boundary ~~was~~ is then applied as

$$v_x(t) = \frac{\Delta V_{right}}{Y(t)\Delta t} = \frac{V_f - V_i}{Y(t) T_{simulation}}, \tag{12}$$

with $Y(t)$ the altitude of the upper right corner of the model. This means both that the time step and the horizontal flow are constant, but this assumption is necessary on a computational point of vue.

The result at the end of the restoration of ~~each~~ the first layer is shown in Fig. 5. As imposed by the boundary conditions, the topography at the end of ~~each layer~~ the restoration is flat, and the fault throw is reduced for all the faults. ~~The restoration behaves well for the first layers, but has more difficulty restoring the oldest layers, which accumulated more deformation: even though the sand and pyrex layers are expected to become increasingly flat during the restoration, they accumulate more folding. Likewise, the silicone diapirs tend to go upwards whereas they are expected to go downwards to flatten the sand/silicone interface. This is due to the model accumulating computation errors, as well as errors coming from the simplifications we made (on the interfaces during the digitization of the model, on the material flowing from the right boundary and on the material properties inside the different layers for example). Another issue~~ An issue, however, with the use of complete kinematic boundary conditions is the resulting over-parameterization of the system, making it prone to over-steps in the velocity if the volume flow is not perfectly balanced. The fixed time step can, for example, result in particles moving out of the model boundary in the advection step because the CFL condition is not met.

To assess the restoration of the layers below the surface, the tomography image taken after the deposition of the last layer is compared to the position of the restored interfaces at this time (Fig. 6). The tomography image is digitized, allowing the computation of the vertical distance $d_{reference}(x)$ between the restored interface and the actual state of the interface (serving as the reference) at that time, with x the position along the horizontal axis. This distance gives a measure of the error in the restoration of each interface. It is shown in Fig. 7, along with the integral of this distance on the horizontal axis, shown in Table 6. ~~Integral, for each interface between two layers of the model, of the distance between the restored interface at the end of the restoration of the first layer, and its actual state at this time, digitized from the corresponding cross-section. The restoration here is done using the kinematic conditions defined in section 4.1. The interface index corresponds to the index of the overlying layer (see Fig. 4). Interface 1 2 3 4 5 6 7 8 9 10 11 12 13 $\int d$ (mm^2) 191 251 258 289 207 223 178 174 188 177 181 157 130~~

Using these results, we see that the error is overall less than 4 mm~~, which is acceptable considering the size of the model (52 × 263 mm) and the accuracy of the cross-section digitization (around 1 mm)~~. The largest errors appear at the right boundary, where the new material entering during the restoration is not known, introducing a high uncertainty on the resulting interfaces.

~~Overall, these first results are encouraging, as they show the potential of the creeping flow restoration method when applying it to sedimentary basin analogues. One downfall, however, is that the boundary conditions are not natural, which raises doubts about the physical realism of the resulting strain~~On the one hand, this can be considered acceptable considering the size of the model (52 × 263 mm) and the accuracy of the cross-section digitization (around 1 mm). One the other hand, it shows that focusing on the restoration of the first layer is already enough to compare the expectations with the restoration results and see errors.

4.2 ~~Upgrading the kinematic conditions to~~ Choosing more natural ~~boundaries~~boundary conditions

This section aims at ~~improving the unphysical~~ trying to remove the kinematic condition to get more natural right and top boundary conditions. Indeed, in the previous subsection, the ~~right~~ top surface was set to flattening, which induces external forces applied to the free surface. Moreover, the right lateral boundary was considered as having a constant flow, ~~where the flow should in principle depend on the altitude. Moreover, the top surface was set to flattening although it corresponds to a free surface~~determined from the top of the tomography images because it was not known inside the model. However, the lateral flow may vary vertically along the boundary.

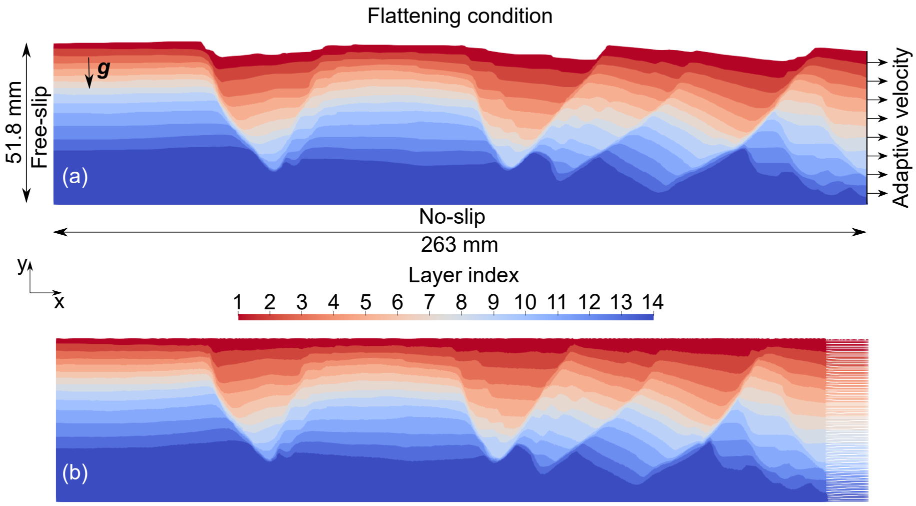

Figure 5. ~~Results~~ Result of the restoration of the ~~successive layers~~ first layer of the analogue model. In this case, the ~~bottom and~~ left ~~boundaries have~~ boundary has a free-slip condition, the bottom boundary is set to a no-slip condition, the top is flattened to the topography height at layer deposition, and the right boundary has a velocity condition which adapts to the flattening condition, based on Eq. (12). (a) shows the setup at the beginning, and (b) ~~to (h) show~~ shows the state of the model at the end of the restoration~~of each layer~~.

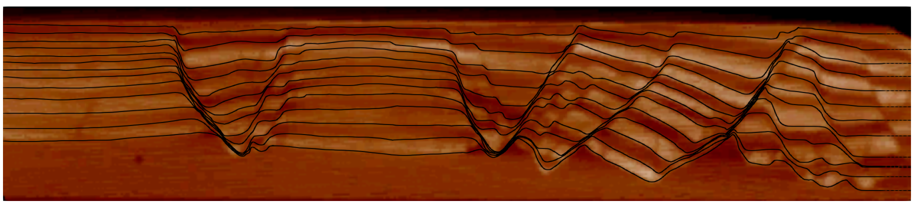

Figure 6. Comparison between the cross-section image taken by X-ray tomography after the deposition of the last layer (shown in background), and the restored interfaces at that time (shown as superimposed black lines). The restoration here is performed using the kinematic conditions defined in section 4.1.

4.2.1 Relaxing the right boundary condition

~~In order to~~ First, we focus on the right boundary condition, leaving the top boundary condition with the top surface flattening described in the previous section. To remove the over-parameterization of the model~~and add more natural boundary conditions, one can change the right boundary condition to a Neumann traction conditioninstead of a Dirichlet velocity condition.~~, we want to replace the Dirichlet condition imposing velocity by a force condition. Indeed, during the laboratory experiment, the right-hand side is open, and the model extends freely by flowing with the action of gravity, so the extension front goes further all through the experiment. The scope of the numerical simulations, however, has a fixed extension in time as it focuses on the part where the tomography images were taken. Following Gunzburger and Cornet (2007), we assume that the effective condition applied on the right boundary of the numerical model stems from the weight of the overlying material, part of which is transfered horizontally under a static equilibrium assumption. The weight of the materials on the right side of the model can then be accounted for by introducing a traction based on the pressure on the right boundary. Here, the traction we use is based on the lithostatic pressure $p(x,y)$ inside the model:

$$p(x,y) = p_0 + \int_{y}^{y_{max}(x)} \rho(x,y)||\boldsymbol{g}||y dy, \qquad (13)$$

with p_0 the pressure at the top surface of the model (neglected here after). In the case of ~~our~~ the analogue model, we consider a constant gravity vector $\boldsymbol{g}$ and the density as constant in each layer, which makes the lithostatic pressure piecewise linear (Fig. 8). The Neumann traction condition applied on the right boundary is then defined as:

$$\boldsymbol{h}_N(y) = -\cancel{\nu}\frac{\nu}{1-\nu} p(x_{max},y)\boldsymbol{n} \qquad (14)$$

where the Poisson coefficient is taken as ~~$\nu_{overburden} = 0.4$~~ $\nu_{overburden} = 0.29$ in the sand and pyrex layers and ~~$\nu_{silicone} = 0.5$~~ $\nu_{silicone} = 0.33$ in the incompressible silicone layer, and $\boldsymbol{n}$ is the outward unit normal vector of the right border. This approximation of the traction and

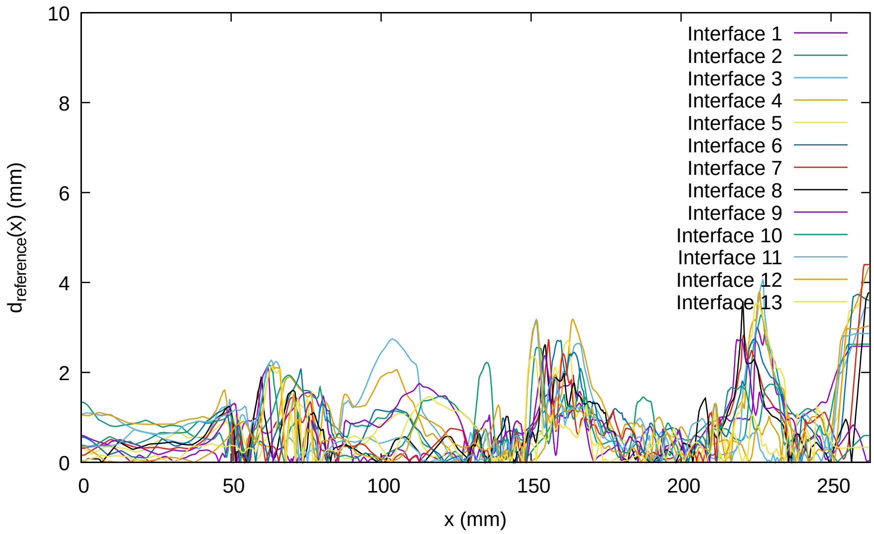

Figure 7. Distance (in absolute value), for each interface between two layers of the model, between the restored interface at the end of the restoration of the first layer, and its actual state at this time, digitized from the corresponding cross-section. The restoration here is performed using the kinematic conditions defined in section 4.1. The interface index corresponds to the index of the layer directly above, starting with interface 1 being the uppermost sand/pyrex interface (see Fig. 4). The digitization of the cross-section has an accuracy of around 1 mm.

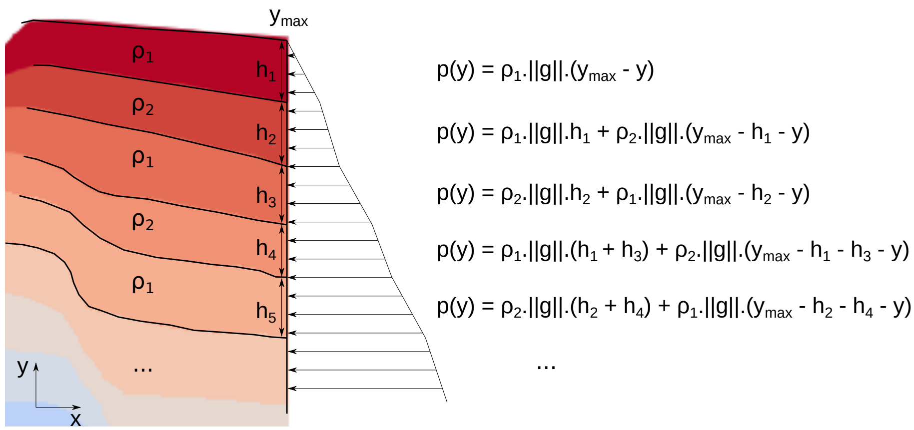

Figure 8. Computation of the lithostatic pressure at the right boundary of the analogue model. A $\cos(\theta)$ factor is then added to the value to take into account the impact of the model tilt on the boundary.

Poisson coefficient values come both from the litterature (e.g., Gunzburger and Cornet, 2007), and tests on various tractions applied at this boundary to find an adequate one.

The results for the successive restoration of the layers with this traction are not shown, as they are similar to those in Fig. 5. However, we show in Fig. 9 shows the distance between the restored interface at the end of the restoration of the first layer and the actual state of the interfaces at that time, along the horizontal axis. The integral of this distance along the horizontal axis is also computed . Integral, for each interface between two layers of the model, between the restored interface at the end of the restoration of the first layer, and its actual state at this time, digitized from the corresponding cross-section. The restoration here is done using the Neumann condition defined in Eq. (14) on the right boundary. The interface index corresponds to the index of the layer directly above, from the indexation of Fig. 4. Interface 1 2 3 4 5 6 7 8 9 10 11 12 13 $\int$d (mm^2) 211 293 313 346 264 289 245 242 264 247 240 193 207 and shown in Table 6.

While imputing this new condition on the right boundary removes the kinematic condition and gives it more physical sense, it also increases the freedom of the model and its sensitivity to the material properties. The slight increase of the error in the restoration of the interfaces, as compared to the fully kinematic boundary conditions, could then come from inaccurate material properties inside the model. This hypothesis is also supported by the following results.

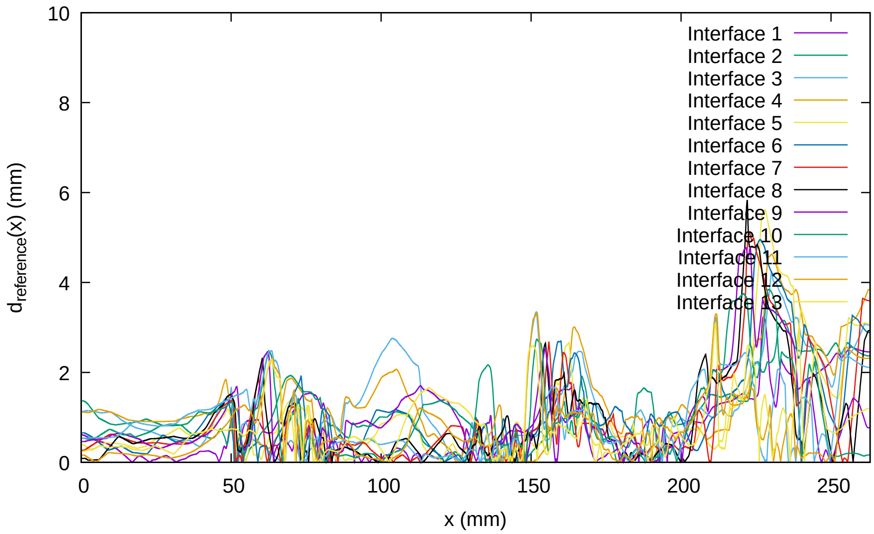

Figure 9. Same as Fig. 7 with the Neumann condition defined in Eq. (14) on the right boundary.

4.2.2 Relaxing the ~~top~~ free surface condition

In the previous simulations, the goal was to test if the model could be restored with creeping flow simulations and a classical topography flattening boundary condition, and to estimate the impact of the lateral boundary condition. While it makes the top surface go back to the state it was at deposition time, ~~it is unphysical~~ its physical behavior is highly questionnable (Lovely et al., 2012). Indeed, as the topography of the model is in contact with air during the analogue experiment, a free surface condition ~~should be set on it~~seems more natural. Moreover, flattening means imposing a Dirichlet condition, but the velocity of the topography through time is not known, so an assumption has to be made (we here ~~assume~~ assumed a constant velocity). Enforcing a velocity condition also makes it unsure wether the other model parameters are relevant or if they just scale well with the imposed deformation. ~~For example, Fig. 10 shows the top surface of the model after some time steps, when it is treated as~~ Here, we test the impact of having a free surface ~~(i. e.~~ condition on the top boundary. For this, two restoration configurations were used (the left and bottom boundary conditions being the same as in the previous sections): one with the Dirichlet condition shown in Section 4.1 and one with the Neumann condition of the previous of Section 4.2.1. In these simulations, only gravity and the right boundary condition drive the deformation~~)~~. Fig. 10 shows the top surface of the model after around 15 minutes of restoration, in these two configurations. We can see that imposing the traction ~~14~~ (14) on the right boundary condition is necessary to balance the model properly, or the topography becomes steeper instead of becoming flat during the ~~deformation~~restoration. When the condition on the right boundary is set to a traction based on the lithostatic pressure, the fault throws of all the faults are reduced during the simulation, and the topography comes closer to being flat. While this balance is encouraging, the model is ~~still not~~ far from being restored properly, as the model deformation is not consistent with the analogue experiment, where the velocity is lower. ~~This is due to~~ Too much material is added during the restoration, and the restored horizon is almost universally above the horizontal datum. This shows that removing the kinematic boundary conditions alone is not enough to properly restore a model. The following Section will discuss the impact of the material properties~~inside the model being incorrect, and particularly the sand and pyrex viscosities being too low~~, and how they can be improved to obtain better restoration results while keeping boundary conditions which do not enforce velocity.

5 Model material parameters analysis

5.1 Rough estimation of the material properties

In the previous section, the impact of the boundary conditions on the restoration of the analogue model was discussed. It ~~suggested~~ showed that removing all kinematic boundary conditions introduced an overestimation of the amount of material entering the model during the restoration. Here, we suggest that finding relevant effective material properties ~~was~~ is necessary to improve the restoration process. In this section, the material properties that come from the data ~~(shown in the grey cells of Table 4)~~ are considered as known and we look for the effective viscosity of the sand and pyrex layers. The boundary conditions are set as shown in Fig. 11. The left boundary is set to a free-slip condition; the bottom boundary is set to a no-slip condition; the right boundary uses the Neumann traction condition defined in Eq. (14); the top bound-

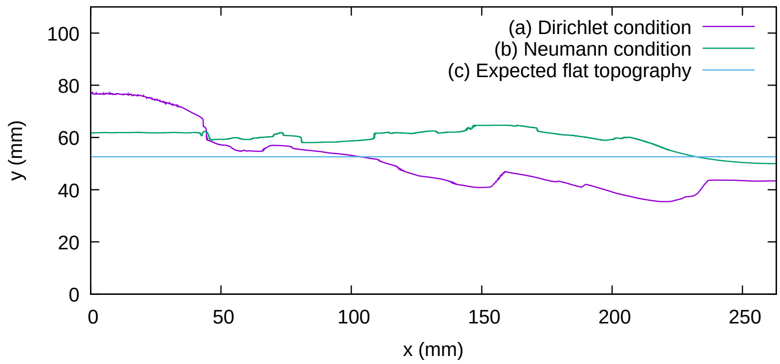

Figure 10. Impact of the boundary conditions on the top surface topography, after ~~a few hundred time steps~~ around 15 minutes of restoration. The bottom and left boundaries have a free-slip condition and the top is a free surface. The right boundary condition is either (a) a constant flow based on Eq. (12) or (b) the Neumann condition defined in Eq. (14). The expected flat topography is given in (c) as a reference. We see that unphysical Dirichlet condition deforms the topography by bringing up the left part of the model and bringing down the right part of the model. On the contrary, using the traction based on the lithostatic pressure, the whole model is brought up and the fault throws are reduced. We can see, however, that the material properties inside the model do not restore it properly: the top surface ends up higher than expected.

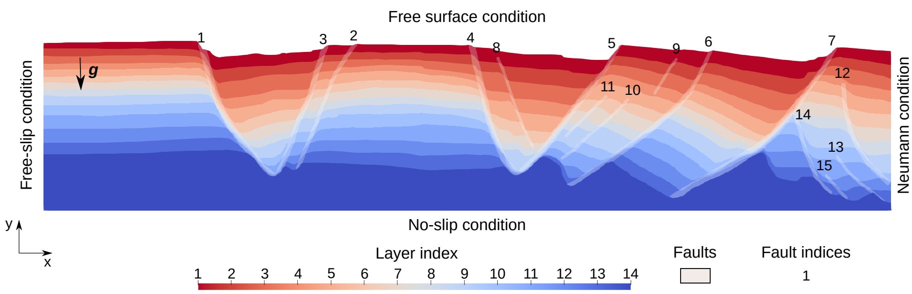

Figure 11. Setup of the analogue model to assess the impact of the material properties on the restoration simulations. The right boundary uses the Neumann condition defined in Eq. (14).

ary condition is set to a free surface. Doing so, the impact of the choice of material properties on the simulation can be assessed without enforcing the velocity on any boundary.

As most of the material properties are given as data, only the viscosity of the sand and pyrex layers are left as unknowns. For simplicity, the viscosity is considered as homogeneous in each layer (outside the faults), with the same value in all the layers no matter whether they are in sand or pyrex. In the faults, the applied viscosity is minimal at the core and increases with a power law up to the contact with the rest of the layers. The range of the viscosity of the sand and pyrex (hereafter called "overburden viscosity") is chosen as $[10^5 : 10^7]$ Pa.s~~, in order to have a~~. The viscosity ratio between the silicone and the overburden ~~in the range of $[2 : 2.10^2]$~~ is then between 2 and 2.10^2. The range of the fault viscosity is chosen as $[5.10^3 : \eta_{overburden}/2]$ Pa.s. Eight experiments are conducted, following the parameter choice shown in Fig. 12 for the viscosity of the overburden and faults.

To check the quality of the restoration for each experiment, various criteria can be applied. Here, ~~the implemented criterion~~ we use the expected topography at the end of the restoration of the first layer as a reference. Indeed, it corresponds to the time in the laboratory experiment where the last layer was deposited (18 minutes according to Table 2), so for the model to be restored properly the topography should be flat and at a specific altitude at this moment. The implemented criterion then corresponds to the area between the topography of the model at any point x in the restoration and ~~the expected topographyafter the restoration of the first layer~~this reference topography. It allows a tracking and comparison of the results throughout the simulation. It is computed as:

$$C_{expected\ horizontality}(t) = \int_{0}^{x_{max}} |y_{top}(x,t) - y_{expected}|\, dx, \tag{15}$$

where x_{max} is the domain length, $y_{top}(x,t)$ is the altitude of the topography along the x axis at a given time t, and $y_{expected}$ is the expected altitude of the topography at the end of the restoration of the layer (from Table 2). This crite-

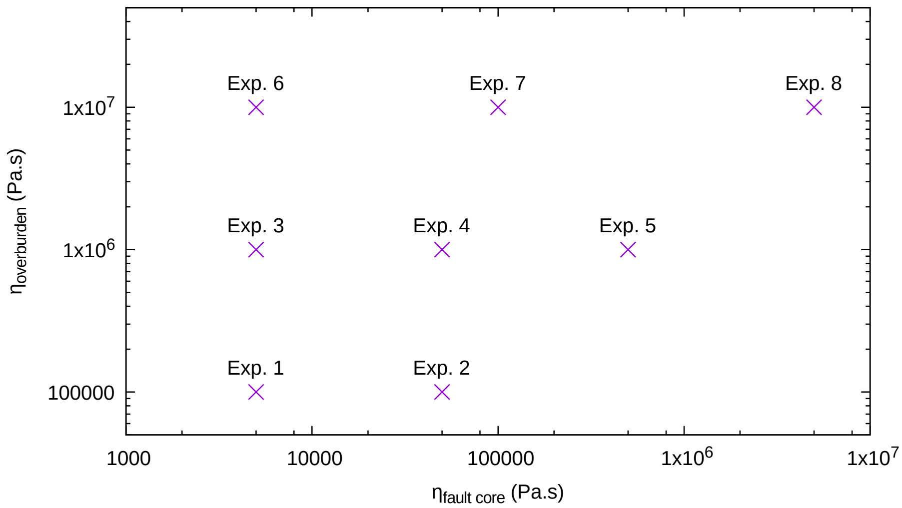

Figure 12. Design of experiments to estimate the effective material properties of the analogue model.

rion is hereafter referred to as the expected horizontality criterion. It has several advantages: first, it is relatively simple to compute and track throughout the restoration simulations. Second, it gives a value of the global difference between the model and the expected restoration result with a flattened top layer. Third, it can be used to compare simulations which evolve at different velocities, and to check when they start to evolve in the wrong direction (i.e., creating relief in reverse time).

The values of the expected horizontality criterion through time for the eight experiments are given in Fig. 13. The results are shown for 18 minutes, which corresponds to the restoration of the first layer (Table 2). In all the experiments, we can see that the model deformation starts by going towards a flat topography at the expected altitude (the expected horizontality criterion decreases towards zero). In experiments 1 to 3, after some time this behavior changes and the model topography evolves away from the expected altitude. In the other experiments, the expected horizontality criterion decreases, but does not reach zero before the end of the layer restoration. In experiments 1 to 3, we let the simulations continue after the criterion started to increase, for testing purposes. Such an increase could, in practice, be used to detect when a restoration simulation is wrong (because of computational instabilities like those shown present in Section 4.2.2 with a Dirichlet condition on the right boundary for example) and to stop the simulation.

While the expected horizontality criterion is good to determine the global distance between the simulations and the expected result, it is not enough to determine the 'best' material parameters for the restoration. Figures 14 and 15 show the state of the model for each experiment at the time t_{final} of their last point in Fig. 13, in order to analyze the impact of each parameter involved in the design of experiments in a more detailed way.

In experiments 1 and 2, the rapid increase of the expected horizontality criterion is explained by the right part of the model going up. The overall restoration also shows that the thicknesses of the overburden layers increase too much, while the fault throws are not reduced much during the simulation. It can be explained by the viscosity of the overburden being too low as compared to the viscosity of the faults. In experiment 3, we observe that the fault throws are overall reduced, but some of them get inverted (on faults 2, 6 and 7, with the numbering of Fig. 4), suggesting that the viscosity of these faults is too low. In experiment 4, as in experiments 1 and 2 (but not in the same proportions), the deformation of the left and right parts of the model is a bit strong, while the fault throws are not reduced much, showing that the viscosity of the faults is not low enough, while the viscosity of the overburden is too low. In experiment 6, the fault throws are overall reduced or canceled. Although it shows the smallest value of the expected horizontality criterion (Fig. 13), faults 2, 6 and 7 (with the numbering of Fig. 4) start to invert their throw, like in experiment 3, showing that their viscosity is too low as compared to the viscosity of the overburden. In experiments 7 and 8, the overall deformation is too small, showing that the viscosity of both the overburden and faults is too high.

The results of these experiments show that it is possible to narrow down the possible values of the effective parameters in this type of model. It also shows, however, that the viscosity of the materials at play cannot be modeled by a unique value for all the material types. Particularly, the viscosity should differ imposing the same viscosity on all the faults seems like a wrong assumption. Indeed, fault histories and mechanical properties differ in the experiment as in real

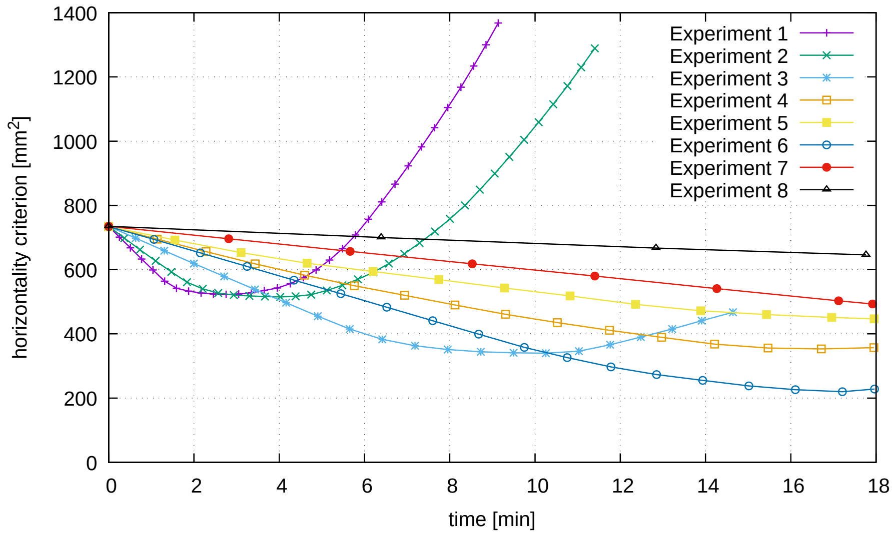

Figure 13. Values of the expected horizontality criterion (Eq. (15)) throughout time for the simulations of the design of experiments (Fig. 12) to find the effective material properties inside the analogue model.

geological settings. In the following, we try to improve the simulations by imposing a different viscosity from one fault to the other: as their histories differ, so do their mechanical properties.

5.2 Fine tuning of the material parameters

Given the previous results, the viscosity of the faults looks like an important parameter to improve restoration. More specifically, the fault inversion appearing only on some faults in experiments 3 and 6 calls for a specific treatment of each fault. In the following, we carry out tests to estimate the viscosity within each fault. The material properties that were considered as known in the previous section do not change (see the grey cells of Table 4). Based on the previous results, the viscosity in the overburden layers is set to 8.10^6 Pa.s, and the default viscosity at the core of the faults is set to 5.10^3 Pa.s (close to their value in Experiment 6). Starting from this default value, various tests are performed by multiplying it by different factors (from 0.75 to 3) in each fault. The factors which give the best restoration results are shown in Table 5. For this restoration, the values of the expected horizontality criterion as a function of time are compared to previous results (Fig. 16). They show that a finer analysis of each fault fine tuning of fault properties upgrades the global restoration and makes the model closer to being flat at the end of the restoration simulation. In order to look at a more global criterion, Fig. 17 shows the comparison between the tomography image taken after the deposition of the last layer and the position of the restored interfaces at this time. Additionally, Fig. 18 shows, for each layer interface, the vertical distance between the restored interface and the actual state of the interface at that time, along the horizontal axis. The integral of this distance along the horizontal axis is given in Table 6. Overall, the analysis of the restored interfaces yields lower restoration errors than with fully kinematic boundaries. Both the visual (Fig. 17) and quantitative comparisons of the X-ray tomography image and the restored interfaces show that the restoration is better on most of the interfaces. The highest errors come from the faults, where the low viscosity induces a "squeezing" effect on the material inside the shear band during the simulation, resulting in an upward motion at their position, particularly near the top of the model.

These results show that it is possible to obtain slighly better restoration results than those obtained with kinematic conditions, while also being more physical and giving by removing kinematic boundary conditions, replacing them with more natural conditions. This, however, passes by a long analysis of the material parameters to find some that are as close as possible to the effective ones. While this process gives valuable information on the effective viscosity to apply in numerical simulations of viscous-based models, it also shows that restoration with "natural" boundary conditions is not as simple to obtain as one would hope.

6 Discussion

Previous restoration approaches have shown that geomechanical schemes can be used to add physical meaning to the restoration process (e.g., Maerten and Maerten, 2001; Muron, 2005; Moretti et al., 2006; Durand-Riard et al., 2010; Chauvin et al., 2018), and account for specific rheological behavior such as that of salt rock (e.g., Kaus and Podladchikov, 2001; Ismail-Zadeh et al., 2001, 2004). Recently, Schuh-Senlis et al. (2020) showed that creeping flow restora-

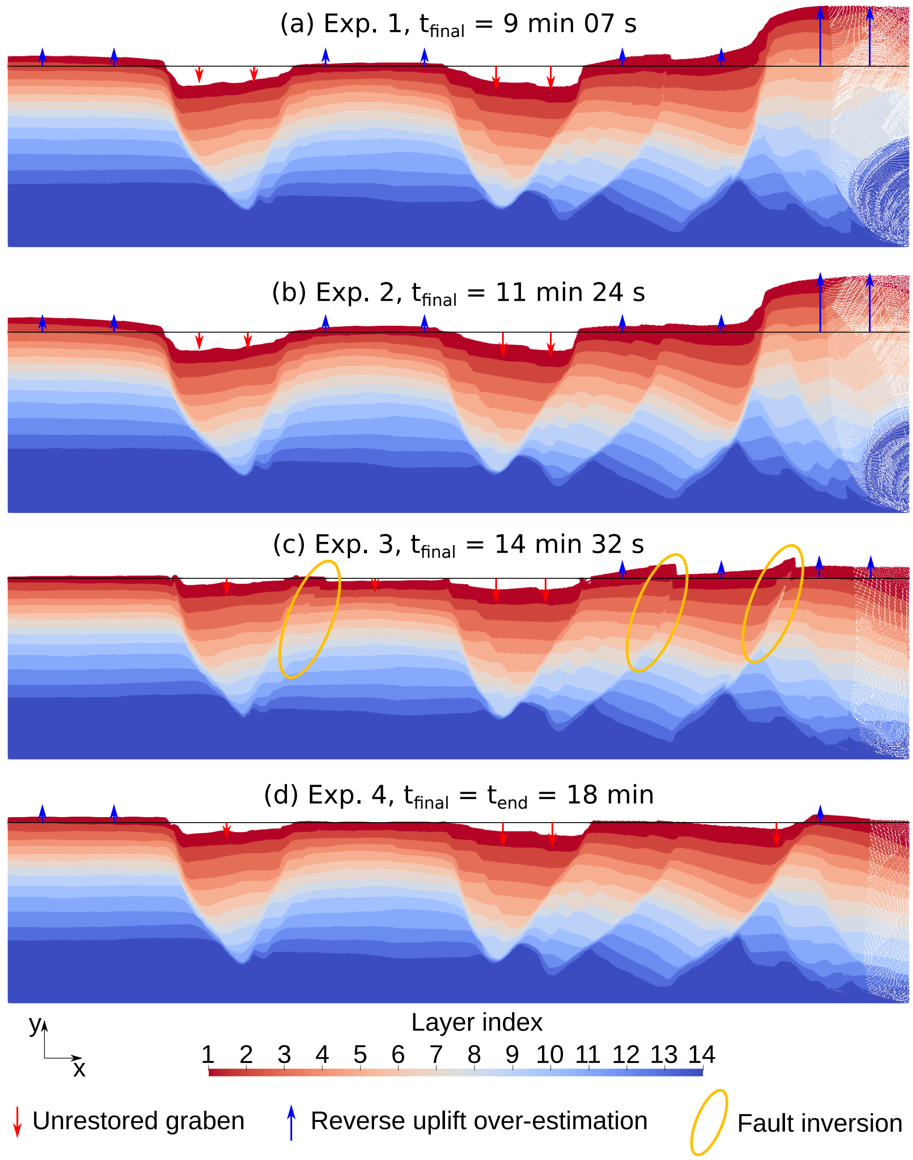

Figure 14. Results of experiments 1 to 4 (Fig. 12) to find the effective material properties inside the analogue model. For each experiment, t_{final} is the restoration time at which the simulation is stopped, and for which the model is shown. t_{end} is the time at the end of the restoration of the first layer. The black line on each result is the expected position of the topography at the end of the restoration of the first layer.

Table 5. Factors to multiply the default fault core viscosity to obtain the best restoration result in Section 5.2. The fault indices are defined in Fig. 4.

Fault index	1	2	3	4	6	7
Multiplying factor	0.75	7	3	2	7	3

tion could be applied to synthetic basin models which include salt, faults and a free surface condition at the top. To go further, we here applied the restoration process of Schuh-Senlis et al. (2020) to an analogue experiment model. This allowed us to test the results of the creeping flow restoration method on a model obtained by the deformation of an actual material, specifically one (sand and pyrex) that is not ideally represented as a Newtonian fluid. The deformation history images on a cross-section were used to quantify the accuracy of the restoration results, and some reference rheological values of the laboratory analogue experiment (e.g., ~~salt~~ silicon viscosity) were introduced in the numerical model to make our test simpler.

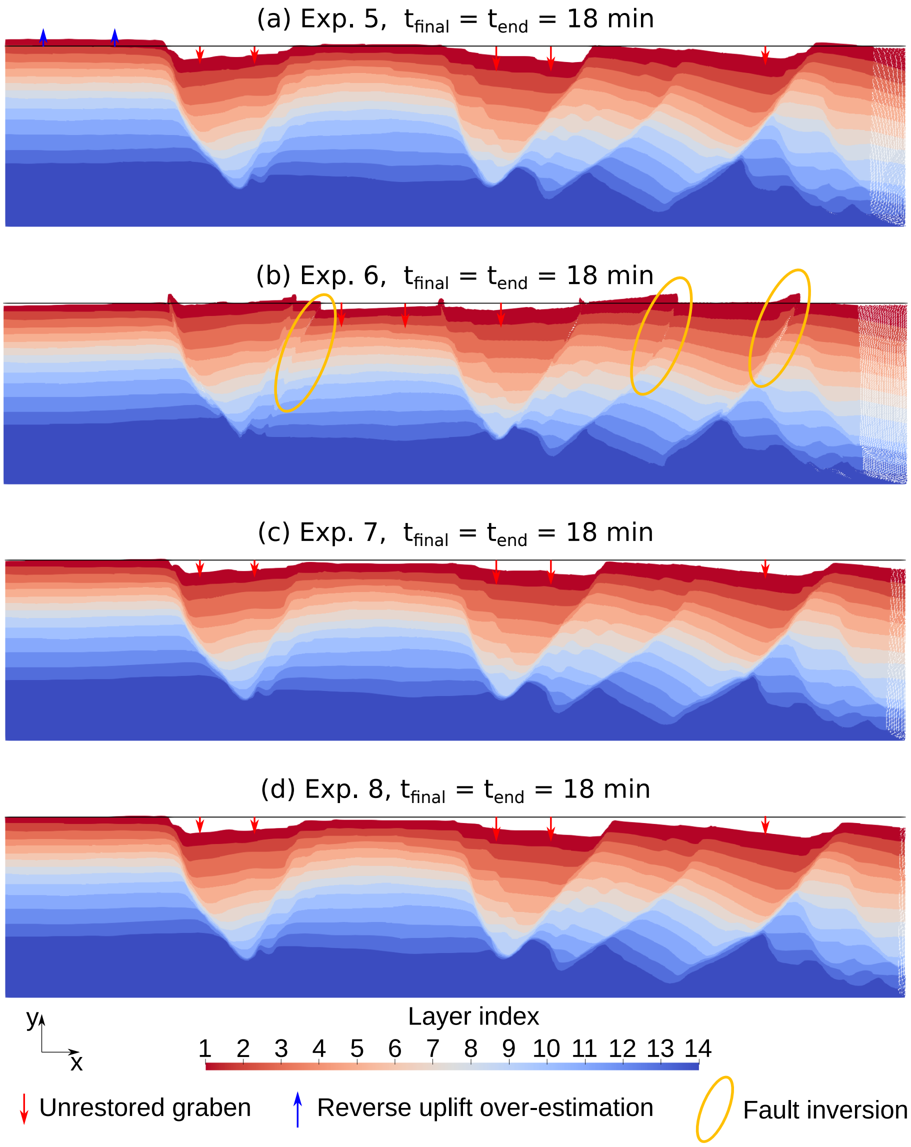

Figure 15. Same as Fig. 14 for experiments 5 to 8.

~~In the analogue model on which the restoration method is applied, the viscosity is as low as 5.10^3 Pa.s and time-scales range from seconds to hours.~~ While neglecting the inertial part of the Navier-Stokes equations ~~at these scales~~ in simulations at the scale of the analogue model is questionnable, this hypothesis is supported by three points. First, the displacement during the experiment is sufficiently slow to neglect any inertial effects. Second, the restoration results back up this assertion. Third, this is a limit-case to test the validity of the method on an analogue experiment, and the application on the corresponding geological model would verify the same hypothesis, as stated in Sect. 2.1.1.

The first tests on the analogue experiment model showed that the first ~~layers~~ layer of the model could be restored properly with kinematic boundary conditions such as those used in standard geomechanical restoration. ~~More natural~~ Other boundary conditions were then tested to remove the kinematic part of the conditions, namely a Neumann traction condition on the right boundary, which accounts for the lithostatic pressure, and a free surface condition on the top surface of the model. ~~Some~~ While these boundary conditions seem to better reflect the tectonic settings, the erratic results obtained ~~with these more realistic boundary conditions suggest that they can~~ suggested that changing the boundary conditions alone was not enough to restore the model properly. They also suggested, however, that they could be used to detect errors in some model parameters (e.g., other boundary conditions or material properties). When building on this error detection to find more appropriate material properties, it was

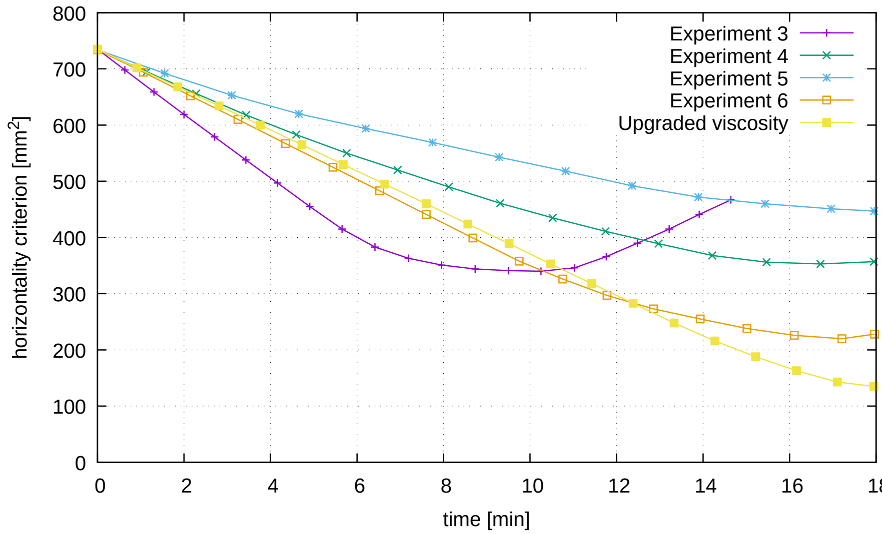

Figure 16. Values of the expected horizontality criterion (Eq. (15)) through time for the restoration with a fine tuning of the fault viscosity (yellow curve), as compared to some experiments of Section 5.1.

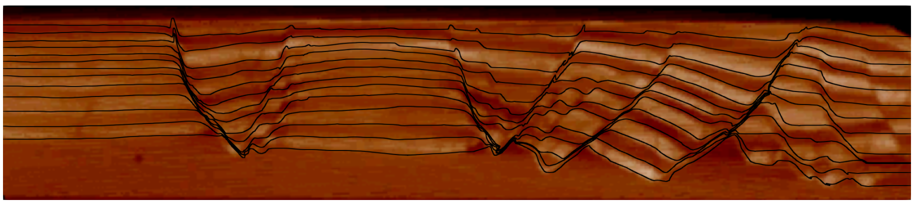

Figure 17. Comparison between the cross-section image taken by X-ray tomography after the deposition of the last layer (shown in background), and the restored interfaces at that time in the restoration process (shown as superimposed black lines). The restoration here is done using the boundary conditions and model parameters of section 5.2.

shown that the restoration results could even be improved, albeit slightly, despite removing all kinematic conditions.

The case of the left and bottom boundaries has not been discussed much. The ~~first tests (Section 4)~~ tests used a free-slip condition on ~~both surfaces, and the simulations in the design of experiments (Section 5) changed the bottom boundary to~~ the left boundary and a no-slip condition ~~. These~~ on the bottom boundary, but these assumptions are simplifications, and a friction condition on the bottom and a Neumann condition on the left-hand side might be more physical. Several tests showed, however, that the difference between a free-slip and no-slip condition on the two boundaries ~~impacted~~ impact the simulations only if they ~~were~~ are otherwise unbalanced (by a wrong traction on the right boundary, for example).

For the right boundary~~traction,~~ , our static equilibrium assumption entails that the traction applied depends directly on the Poisson coefficient~~was set~~ . In our study, we set this coefficient from reference values for the type of granular material in the model, but ~~it~~ its impact may have to be estimated more properly and more precisely. Indeed, additional tests have shown that while the Poisson coefficient value does not impact the general behavior of the model, it can impact the value of the 'best' effective viscosity inside the model. Another possible issue with the traction at the right boundary of the model is the account of the tilt and its implications on the material on the other side of the boundary. Here, we did not consider the impact of the movement of this material, as the Stokes equations ignore the inertia of the ~~model~~material. It poses, however, the following question: does the movement of surrounding materials impact the horizontal pressure applied by them on the boundaries of the model ? In which case, the traction would have to be changed accordingly.

The tests done on the boundary conditions of the analogue experiment model also showed that when no kinematic condition was applied, the material properties ~~used at this point did~~ initially assumed do not allow the restoration of the model. To study their impact and to find the 'best' effective properties inside the model, a design of experiment was used, and the restoration scheme was applied to eight models with different properties. As the viscosity of the silicone and the density of all materials were known, the parameters we studied were the viscosity inside the faults and the viscosity in the sand and pyrex layers. The first experiments helped nar-

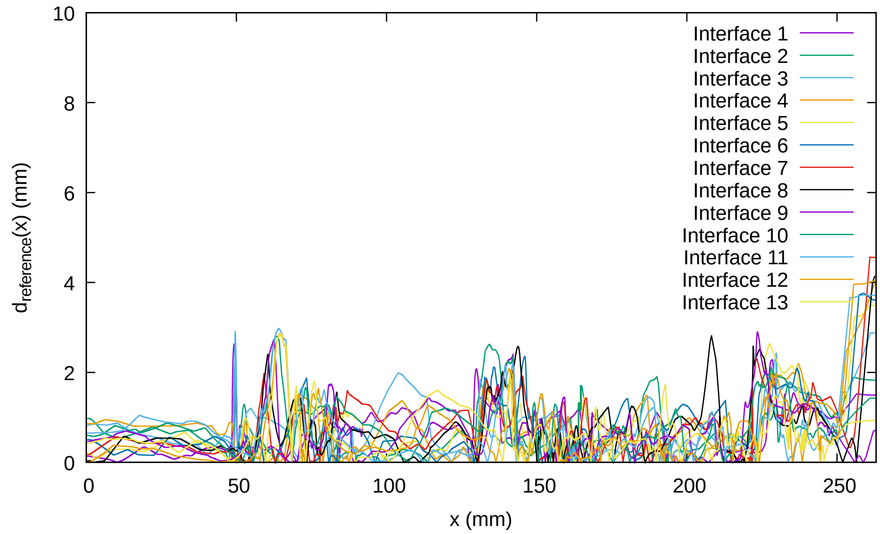

Figure 18. Same as Fig. 7 with the boundary conditions and model parameters of section 5.2.

Table 6. Integral, for each interface between two layers of the model, of the distance between the restored interface at the end of the restoration of the first layer, and its actual state at this time, digitized from the corresponding cross-section. The In the first line, the restoration here is done using the kinematic conditions (flattening on top and dirichlet condition on the right) defined in Section 4.1. In the second line, the restoration is done using the conditions defined in Section 4.2.1 (flattening on top and the Neumann condition defined in Eq. (14) on the right boundary). The values of In the same distance computed for last line, the restorations of sections 4.1 restoration is done using a free surface on top and 4.2.1 are reminded, for comparisonthe Neumann condition defined in Eq. (14) on the right boundary. The interface index corresponds to the index of the layer directly above, from the indexation of Fig. 4.

Interface index	1	2	3	4	5	6	7	8	9	10	11	12	13	Total
$\int d$ (mm^2) (Free boundaries & effective parameters) 170 190 203 225 189 198 200 196 178 204 200 174 165 2492 $\int d$ (mm^2) (Kinematic restorationOnly Dirichlet conditions)	191	251	258	289	207	223	178	174	188	177	181	157	130	2604
$\int d$ (mm^2) (Flattening & Neumann)	211	293	313	346	264	289	245	242	264	247	240	193	207	3354
$\int d$ (mm^2) (Free top, Neumann right boundary conditions & effective parameters)	170	190	203	225	189	198	200	196	178	204	200	174	165	2492

row down the range of values for these effective viscosities, and showed that a different effective viscosity has to be used for each fault in the model. Various experiments then allowed us to tune the viscosity inside the faults accordingly, and decrease the restoration error. This viscosity tuning, however, was done manually and we could not find a relation between the viscosity difference between the faults, and their difference in age or shear band thickness. More tests using a local criterion on the fault throw for each fault may then be necessary to find how to guide the choice of the fault effective viscosity.

In order to add yet more physics, other simplifications could be lifted, which would require further tests to assess the impact of their removal. For example, we considered the viscosity as independent from time and from the layering of the model. It The hypothesis of a viscous fault behavior could also be revisited in further studies. The consideration of frictional fault surfaces might be considered, but this would compromise the reversibility assumptions used in restoration methods to-date. Another option for future investigations could be to consider time-varying viscosity, to decrease fault viscosity down to that of the intact rock when the fault displacement reaches zero. Along the same lines, it could be interesting , however, to study the influence of accumulated strain (by considering the sand and pyrex layers as visco-elastic materials) or of a variable viscosity in the layers (depending on the type of layer, or on the age and altitude, for example).

An issue that remains to be adressed is the fact that a lower viscosity inside the faults can lead to over-estimations of the horizontal velocity for the faults. In restoration simulations, this leads to the material inside some of the faults being pushed out by the blocks with higher viscosities on the sides. The application of an anisotropic viscosity may remove this issue, but has not been studied yet.

To further assess the creeping flow method potentialuse of creeping flow restoration without kinematic conditions, it would also be interesting to apply it to other structural models. The use of other analogue experiment setups, first, would allow to check the validity of the conditions that were found on this onein this paper. It would also provide the effective properties in a wider range of model deformation types. The comparison of the effective viscosity in different analogue models, for example, could provide interesting data when scaling the effective properties to apply the method on models of the subsurface at geological time scales.

While adding more physical conditions to geomechanical restoration is interesting in itself, the goal is also to provide a working method for the restoration of models describing the subsurface in real cases. Several questions would then arise. First, the scope of this study was set on the restoration of a 2D cross-section. This not only neglects the out-of-plane displacement, but also reduces the scope of the boundary conditions and material properties study. It is unsure, for example, how the viscosity of faults would have to vary lateraly in a 3D model, to be able to restore them properly. Second, the boundary conditions may be more complicated, with the addition of continuous erosion and sedimentation on the topography (compared to punctual sedimentation in the analogue experiment). The forces at play several kilometers deep in the underground are also unknown, and the bottom boundary may be more complex than the free-slip and no-slip conditions applied here. For example, specific flow due to uplift or subsidence of the layers below the model may need to be taken into account. The pressure applied on the lateral boundaries may also prove to be more challenging than a Neumann traction based on the horizontal report of the lithostatic pressure (in which, by the way, uncertainty on the Poisson coefficient value can be large). Indeed, other sources may have an impact on the applied pressure, such as a higher altitude or denser material near the boundaryin heterogeneous media with variable density and mechanical properties. Finally, the space of material parameters to be estimated would be much bigger than that of an analogue experiment model. It would then be useful to find a way to scale the effective parameters from those that were found in analogue experiments with deformation mechanisms analogue to the real-case models. Interestingly, to answer these questions, creeping flow restoration could be a useful tool, because the conditions that best balance the models could be determined as the solution of an inverse problem on the restoration results, using the flattening condition as a likelyhood likelihood metric.

7 Conclusions

In this paper, we have shown the results obtained with the creeping flow restoration method on a complex structural model including various structural model obtained from a laboratory scale analogue model and including multiple faults. The first results start with fully kinematic boundary conditions, showing show that conclusive results can be obtained while changing the consideration of salt layers and faults to a more physical behavior, compared to previous geomechanical restoration schemes using elastic behavior. In order to go further, other boundary conditionswere introduced. While the deformation is then *a priori* more physical, these conditions with classic kinematic boundary conditions. The study then aimed at removing the kinematic part of the boundary conditions to leave more freedom to the modelvelocity, and as such are more sensitive to the material parameters, and assess the impact on the restoration results. It showed that when replacing kinematic conditions with force conditions closer to those of the actual tectonic settings, the model could not be properly restored without material parameters as close as possible to the effective ones.

Using these boundary conditions, however, it was possible to assess the impact of changing the material properties inside the model. By going closer to the effective material properties, we were then even able to obtain results better slightly better results than those using kinematic boundary conditions for the restoration. These results , however, both improved both improve the physical meaning of the restoration, and provided provide valuable information on the effective material properties to use in mechanical simulations.

As such, the creeping flow restoration of this analogue experiment model showed shows that this restoration scheme can be applied to complex real-case structural models , as well as some of the additional data that can be obtained from it. It also opened the way to a number of possible tests that could be performed to find out more on relatively complex structural models in 2D, without any kinematic boundary conditions. This, however, implies a complex trial and error process to find the effective material propertiesinside structural models, particularly when applying the method to geological models, without which the restoration process is not possible. We believe that further investigations and numerical tests are needed to progress on physically-based restoration, especially to analyze the trade-offs between geometric uncertainties in the structural model, material behavior law and the associated properties, and boundary conditions.

Author contributions. MSS wrote the paper original version, the software code and ran the numerical experiments. GC and PC provided discussions on the subject, guidance on solving the different problems, and funding for the PhD thesis that allowed this research through the RING-Gocad consortium. All authors contributed to the conceptualization, the design of experiments, the analysis of results, and the editing of the manuscript.

Competing interests. The authors declare that they have no conflict of interests.

Acknowledgements. This project was done in the frame of the RING project, in the GeoRessources laboratory. We would like to thank for their support the academic and industrial sponsors of the RING-GOCAD Consortium managed by ASGA (https://www.ring-team.org/consortium). We would also like to thank Cedric Thieulot for valuable discussions and suggestions on this work.

References

Al-Fahmi, M. M., Plesch, A., Shaw, J. H., and Cole, J. C.: Restorations of faulted domes, AAPG Bulletin, 100, 151–163, https://doi.org/10.1306/08171514211, 2016a.

Al-Fahmi, M. M., Plesch, A., Shaw, J. H., and Cole, J. C.: Restorations of faulted domes, AAPG Bulletin, 100, 151–163, https://doi.org/10.1306/08171514211, 2016b.

Allen, P. A. and Allen, J. R.: Basin analysis: Principles and application to petroleum play assessment, John Wiley & Sons, 2013.

Arndt, D., Bangerth, W., Clevenger, T. C., Davydov, D., Fehling, M., Garcia-Sanchez, D., Harper, G., Heister, T., Heltai, L., Kronbichler, M., Kynch, R. M., Maier, M., Pelteret, J.-P., Turcksin, B., and Wells, D.: The `deal.II` Library, Version 9.1, Journal of Numerical Mathematics, https://doi.org/10.1515/jnma-2019-0064, accepted, 2019.

Arndt, D., Bangerth, W., Davydov, D., Heister, T., Heltai, L., Kronbichler, M., Maier, M., Pelteret, J.-P., Turcksin, B., and Wells, D.: The deal. II finite element library: Design, features, and insights, Computers & Mathematics with Applications, https://doi.org/10.1016/j.camwa.2020.02.022, 2020.

Asgari, A. and Moresi, L.: Multiscale Particle-In-Cell Method: From Fluid to Solid Mechanics, in: Advanced Methods for Practical Applications in Fluid Mechanics, edited by Jones, S. A., chap. 9, IntechOpen, Rijeka, https://doi.org/10.5772/26419, 2012.

Athy, L. F.: Density, porosity, and compaction of sedimentary rocks, AAPG Bulletin, 14, 1–24, https://doi.org/10.1306/3D93289E-16B1-11D7-8645000102C1865D, 1930.

Back, S., Strozyk, F., Kukla, P. A., and Lambiase, J. J.: Three-dimensional restoration of original sedimentary geometries in deformed basin fill, onshore Brunei Darussalam, NW Borneo, Basin Research, 20, 99–117, https://doi.org/https://doi.org/10.1111/j.1365-2117.2007.00343.x, 2008.

Bangerth, W., Hartmann, R., and Kanschat, G.: deal.II – a General Purpose Object Oriented Finite Element Library, ACM Trans. Math. Softw., 33, 24/1–24/27, https://doi.org/10.1145/1268776.1268779, 2007.

Bouziat, A., Guy, N., Frey, J., Colombo, D., Colin, P., Cacas-Stentz, M.-C., and Cornu, T.: An Assessment of Stress States in Passive Margin Sediments: Iterative Hydro-Mechanical Simulations on Basin Models and Implications for Rock Failure Predictions, Geosciences, 9, 469, https://doi.org/10.3390/geosciences9110469, 2019.

Buiter, S. J., Schreurs, G., Albertz, M., Gerya, T. V., Kaus, B., Landry, W., le Pourhiet, L., Mishin, Y., Egholm, D. L., Cooke, M., Maillot, B., Thieulot, C., Crook, T., May, D., Souloumiac, P., and Beaumont, C.: Benchmarking numerical models of brittle thrust wedges, Journal of Structural Geology, 92, 140–177, https://doi.org/10.1016/j.jsg.2016.03.003, 2016.

Chamberlin, R. T.: The Appalachian folds of central Pennsylvania, The Journal of Geology, 18, 228–251, https://doi.org/10.1086/621722, 1910.

Chauvin, B.: Applicability of the mechanics-based restoration: boundary conditions, fault network and comparison with a geometrical method, Ph.D. thesis, Université de Lorraine, 2017.

Chauvin, B. P., Lovely, P. J., Stockmeyer, J. M., Plesch, A., Caumon, G., and Shaw, J. H.: Validating novel boundary conditions for three-dimensional mechanics-based restoration: An extensional sandbox model example, AAPG Bulletin, 102, 245–266, https://doi.org/10.1306/0504171620817154, 2018.

Cobbold, P., Rossello, E., and Vendeville, B.: Some experiments on interacting sedimentation and deformation above salt horizons, Bulletin de la Société Géologique de France, pp. 453–460, 1989.

Cobbold, P. R. and Percevault, M.-N.: Spatial integration of strains using finite elements, in: Strain Patterns in Rocks, edited by Cobbold, P., Schwerdtner, W., and Treagus, S., pp. 299–305, Pergamon, https://doi.org/10.1016/B978-0-08-030273-7.50010-0, 1983.

Courant, R., Friedrichs, K., and Lewy, H.: Über die partiellen Differenzengleichungen der mathematischen Physik, Mathematische annalen, 100, 32–74, https://doi.org/10.1007/BF01448839, 1928.

Crook, A. J., Obradors-Prats, J., Somer, D., Peric, D., Lovely, P., and Kacewicz, M.: Towards an integrated restoration/forward geomechanical modelling workflow for basin evolution prediction, Oil & Gas Sciences and Technology–Revue d'IFP Energies nouvelles, 73, 18, 2018.

Dahlstrom, C.: Balanced cross sections, Canadian Journal of Earth Sciences, 6, 743–757, https://doi.org/10.1139/e69-069, 1969.

de Melo Garcia, S. F., Letouzey, J., Rudkiewicz, J.-L., Danderfer Filho, A., and Frizon de Lamotte, D.: Structural modeling based on sequential restoration of gravitational salt deformation in the Santos Basin (Brazil), Marine and Petroleum Geology, 35, 337–353, https://doi.org/https://doi.org/10.1016/j.marpetgeo.2012.02.009, 2012.

De Santi, M. R., Campos, J. L. E., and Martha, L. F.: A Finite Element approach for geological section reconstruction, in: Proceedings of the 22th Gocad Meeting, Nancy, France, pp. 1–13, Citeseer, 2002.

Dimakis, P., Braathen, B. I., Faleide, J. I., Elverhøi, A., and Gudlaugsson, S. T.: Cenozoic erosion and the preglacial uplift of the Svalbard–Barents Sea region, Tectonophysics, 300, 311–327, https://doi.org/10.1016/S0040-1951(98)00245-5, 1998.

Donea, J., Huerta, A., Ponthot, J.-P., and Rodriguez-Ferran, A.: Arbitrary Lagrangian-Eulerian Methods, volume 1 of Encyclopedia of Computational Mechanics, chapter 14, John Wiley & Sons Ltd, 3, 1–25, https://doi.org/10.1002/9781119176817.ecm2009, 2004.

Durand-Riard, P., Caumon, G., and Muron, P.: Balanced restoration of geological volumes with relaxed meshing constraints, Computers & Geosciences, 36, 441–452, https://doi.org/10.1016/j.cageo.2009.07.007, 2010.

Durand-Riard, P., Salles, L., Ford, M., Caumon, G., and Pellerin, J.: Understanding the evolution of syn-depositional folds: Coupling decompaction and 3D sequential restoration, Marine and Petroleum Geology, 28, 1530–1539, https://doi.org/10.1016/j.marpetgeo.2011.04.001, 2011.

Durand-Riard, P., Guzofski, C., Caumon, G., and Titeux, M.-O.: Handling natural complexity in three-dimensional geomechanical restoration, with application to the recent evolution of the outer fold and thrust belt, deep-water Niger Delta, AAPG bulletin, 97, 87–102, https://doi.org/10.1306/06121211136, 2013a.

Durand-Riard, P., Shaw, J. H., Plesch, A., and Lufadeju, G.: Enabling 3D geomechanical restoration of strike-and oblique-slip faults using geological constraints, with applications to the deepwater Niger Delta, Journal of Structural Geology, 48, 33–44, https://doi.org/10.1016/j.jsg.2012.12.009, 2013b.

Espurt, N., Angrand, P., Teixell, A., Labaume, P., Ford, M., de Saint Blanquat, M., and Chevrot, S.: Crustal-scale balanced cross-section and restorations of the Central Pyrenean belt (Nestes-Cinca transect): Highlighting the structural control of Variscan belt and Permian-Mesozoic rift systems on mountain building, Tectonophysics, 764, 25–45, https://doi.org/https://doi.org/10.1016/j.tecto.2019.04.026, 2019.

Faulkner, D., Mitchell, T., Healy, D., and Heap, M.: Slip on'weak'faults by the rotation of regional stress in the fracture damage zone, Nature, 444, 922–925, 2006.

Fernandez, N.: 2D and 3D numerical modelling of multilayer detachment folding and salt tectonics, Ph.D. thesis, Mainz University, https://doi.org/10.25358/openscience-2916, 2014.

Fletcher, R. C. and Pollard, D. D.: Can we understand structural and tectonic processes and their products without appeal to a complete mechanics?, Journal of Structural Geology, 21, 1071–1088, https://doi.org/10.1016/S0191-8141(99)00056-5, 1999.

Fossen, H.: Structural geology, Cambridge University Press, second edn., 2016.

Gassmöller, R., Lokavarapu, H., Heien, E., Puckett, E. G., and Bangerth, W.: Flexible and Scalable Particle-in-Cell Methods With Adaptive Mesh Refinement for Geodynamic Computations, Geochemistry, Geophysics, Geosystems, 19, 3596–3604, https://doi.org/10.1029/2018GC007508, 2018.

Gassmöller, R., Lokavarapu, H., Bangerth, W., and Puckett, E. G.: Evaluating the accuracy of hybrid finite element/particle-in-cell methods for modelling incompressible Stokes flow, Geophysical Journal International, 219, 1915–1938, https://doi.org/10.1093/gji/ggz405, 2019.

Gratier, J.-P.: L'équilibrage des coupes géologiques. Buts, méthodes et applications., Géosciences-Rennes, 1988.

Groshong, R.: 3-D structural geology, Springer, Berlin, Heidelberg, https://doi.org/10.1007/978-3-540-31055-6, 2006.

Gunzburger, Y. and Cornet, F. H.: Rheological characterization of a sedimentary formation from a stress profile inversion, Geophysical Journal International, 168, 402–418, https://doi.org/10.1111/j.1365-246X.2006.03140.x, 2007.

Guzofski, C. A., Mueller, J. P., Shaw, J. H., Muron, P., Medwedeff, D. A., Bilotti, F., and Rivero, C.: Insights into the mechanisms of fault-related folding provided by volumetric structural restorations using spatially varying mechanical constraints, AAPG bulletin, 93, 479–502, https://doi.org/10.1306/11250807130, 2009.

Hall, J.: II. On the Vertical Position and Convolutions of certain Strata, and their relation with Granite, Transactions of the Royal Society of Edinburgh, 7, 79–108, https://doi.org/10.1017/S0080456800019268, 1815.

IFP and C&C Reservoirs: Principles of Digital Structural Analog Modeling, Tech. rep., 2006.

Ismail-Zadeh, A. and Tackley, P.: Computational methods for geodynamics, Cambridge University Press, https://doi.org/10.1017/CBO9780511780820, 2010.

Ismail-Zadeh, A., Tsepelev, I., Talbot, C., and Korotkii, A.: Three-dimensional forward and backward modelling of diapirism: numerical approach and its applicability to the evolution of salt structures in the Pricaspian basin, Tectonophysics, 387, 81–103, https://doi.org/10.1016/j.tecto.2004.06.006, 2004.

Ismail-Zadeh, A. T., Talbot, C. J., and Volozh, Y. A.: Dynamic restoration of profiles across diapiric salt structures: numerical approach and its applications, Tectonophysics, 337, 23–38, https://doi.org/10.1016/S0040-1951(01)00111-1, 2001.

Kaus, B. J. and Podladchikov, Y. Y.: Forward and reverse modeling of the three-dimensional viscous Rayleigh-Taylor instability, Geophysical Research Letters, 28, 1095–1098, https://doi.org/10.1029/2000GL011789, 2001.

Kaus, B. J., Mühlhaus, H., and May, D. A.: A stabilization algorithm for geodynamic numerical simulations with a free surface, Physics of the Earth and Planetary Interiors, 181, 12–20, https://doi.org/10.1016/j.pepi.2010.04.007, 2010.

Kocher, T. and Mancktelow, N. S.: Dynamic reverse modelling of flanking structures: a source of quantitative kinematic information, Journal of Structural Geology, 27, 1346–1354, https://doi.org/10.1016/j.jsg.2005.05.007, 2005.

Kronbichler, M., Heister, T., and Bangerth, W.: High accuracy mantle convection simulation through modern numerical methods, Geophysical Journal International, 191, 12–29, https://doi.org/10.1111/j.1365-246X.2012.05609.x, 2012.

Lechmann, S. M., Schmalholz, S. M., Burg, J.-P., and Marques, F.: Dynamic unfolding of multilayers: 2D numerical approach and application to turbidites in SW Portugal, Tectonophysics, 494, 64–74, https://doi.org/10.1016/j.tecto.2010.08.009, 2010.

Lovely, P., Flodin, E., Guzofski, C., Maerten, F., and Pollard, D. D.: Pitfalls among the promises of mechanics-based restoration: Addressing implications of unphysical boundary conditions, Journal of Structural Geology, 41, 47–63, https://doi.org/10.1016/j.jsg.2012.02.020, 2012.

Lovely, P. J., Jayr, S. N., and Medwedeff, D. A.: Practical and efficient three-dimensional structural restoration using an adaptation of the GeoChron model, AAPG Bulletin, 102, 1985–2016, https://doi.org/10.1306/03291817191, 2018.

Maerten, F. and Maerten, L.: Unfolding and Restoring Complex Geological Structures Using Linear Elasticity Theory, in: AGU Fall Meeting Abstracts, vol. 2001, pp. T22C–0940, 2001.

Maerten, L. and Maerten, F.: Chronologic modeling of faulted and fractured reservoirs using geomechanically based restoration:

Technique and industry applications, AAPG bulletin, 90, 1201–1226, https://doi.org/10.1306/02240605116, 2006.

Massimi, P., Quarteroni, A., and Scrofani, G.: An adaptive finite element method for modeling salt diapirism, Mathematical Models and Methods in Applied Sciences, 16, 587–614, https://doi.org/10.1142/S0218202506001273, 2006.

Massot, J.: Implémentation de méthodes de restauration équilibrée 3D, Ph.D. thesis, Institut National Polytechnique de Lorraine, 2002.

Moretti, I.: Working in complex areas: New restoration workflow based on quality control, 2D and 3D restorations, Marine and Petroleum Geology, 25, 205–218, https://doi.org/10.1016/j.marpetgeo.2007.07.001, 2008.

Moretti, I., Lepage, F., and Guiton, M.: KINE3D: a new 3D restoration method based on a mixed approach linking geometry and geomechanics, Oil & Gas Science and Technology, 61, 277–289, https://doi.org/10.2516/ogst:2006021, 2006.

Muron, P.: Méthodes numériques 3-D de restauration des structures géologiques faillées, Ph.D. thesis, INPL, 2005.

Parquer, M. N., Collon, P., and Caumon, G.: Reconstruction of Channelized Systems Through a Conditioned Reverse Migration Method, Mathematical Geosciences, 49, 965–994, https://doi.org/10.1007/s11004-017-9700-3, 2017.

Ramberg, H.: Gravity, deformation and the earth's crust: in theory, experiments and geological application, London ; New York : Academic Press, 2d ed edn., 1981.

Ramón, M. J., Pueyo, E. L., Caumon, G., and Briz, J. L.: Parametric unfolding of flexural folds using palaeomagnetic vectors, Geological Society, London, Special Publications, 425, 247–258, https://doi.org/10.1144/SP425.6, 2016.

Rouby, D.: Restauration en carte des domaines faillés en extension. Méthode et applications., Ph.D. thesis, Université Rennes 1, 1994.

Royden, L. and Keen, C.: Rifting process and thermal evolution of the continental margin of eastern Canada determined from subsidence curves, Earth and Planetary Science Letters, 51, 343–361, https://doi.org/10.1016/0012-821X(80)90216-2, 1980.

Schmalholz, S. M.: 3D numerical modeling of forward folding and reverse unfolding of a viscous single-layer: Implications for the formation of folds and fold patterns, Tectonophysics, 446, 31–41, https://doi.org/10.1016/j.tecto.2007.09.005, 2008.

Schönborn, G.: Balancing cross sections with kinematic constraints: The Dolomites (northern Italy), Tectonics, 18, 527–545, 1999.

Schreurs, G., Buiter, S. J., Boutelier, J., Burberry, C., Callot, J.-P., Cavozzi, C., Cerca, M., Chen, J.-H., Cristallini, E., Cruden, A. R., Cruz, L., Daniel, J.-M., Da Poian, G., Garcia, V. H., Gomes, C. J., Grall, C., Guillot, Y., Guzmán, C., Hidayah, T. N., Hilley, G., Klinkmüller, M., Koyi, H. A., Lu, C.-Y., Maillot, B., Meriaux, C., Nilfouroushan, F., Pan, C.-C., Pillot, D., Portillo, R., Rosenau, M., Schellart, W. P., Schlische, R. W., Take, A., Vendeville, B., Vergnaud, M., Vettori, M., Wang, S.-H., Withjack, M. O., Yagupsky, D., and Yamada, Y.: Benchmarking analogue models of brittle thrust wedges, Journal of Structural Geology, 92, 116–139, https://doi.org/https://doi.org/10.1016/j.jsg.2016.03.005, 2016.

Schuh-Senlis, M., Thieulot, C., Cupillard, P., and Caumon, G.: Towards the application of Stokes flow equations to structural restoration simulations, Solid Earth, 11, 1909–1930, https://doi.org/10.5194/se-11-1909-2020, 2020.

Stockmeyer, J. M. and Guzofski, C.: Interplay between extension, salt and pre-existing structure, offshore Angola, in: AAPG Annual Convention and Exhibition, 2014.

Tang, P., Wang, C., and Dai, X.: A majorized Newton-CG augmented Lagrangian-based finite element method for 3D restoration of geological models, Computers & Geosciences, 89, 200–206, https://doi.org/10.1016/j.cageo.2016.01.013, 2016.

Thielmann, M., May, D., and Kaus, B.: Discretization errors in the hybrid finite element particle-in-cell method, Pure and Applied Geophysics, 171, 2165–2184, https://doi.org/10.1007/s00024-014-0808-9, 2014.

Trim, S., Lowman, J., and Butler, S.: Improving mass conservation with the tracer ratio method: application to thermochemical mantle flows, Geochemistry, Geophysics, Geosystems, 21, e2019GC008 799, https://doi.org/10.1029/2019GC008799, 2020.

Willis, B.: The mechanics of Appalachian structure, vol. 13, US Government Printing Office, 1894.